RESULTS

Normal Human Diploid Fibroblasts Skip Mitosis in Response to Various Senescence-Inducing Stimuli before Growth Arrest Occurs

In order to directly determine from where senescent cells exit the cell cycle, we performed time-lapse live-cell imaging of asynchronously growing normal human diploid fibroblast (HDF) HCA2 cells transduced with lentiviruses expressing Cdt1 fragment-fused mCherry and geminin fragment-fused AmCyan proteins (Sakaue-Sawano et al., 2008). Imaging was conducted over a 3 day period and included control cells that divide normally (Figure 1A). In contrast to the control cells, 70% of the cells treated with senescence-inducing agents degraded geminin and accumulated Cdt1 without entry into mitosis (Cdt1 switching) (Figure 1B). Imaging allowed us to determine that there were changes in the nucleus that indicated entry into mitosis, such as mitotic rounding and nuclear envelope breakdown. These cells ceased cycling in the 3 day observation time. The rate was somewhat lower in cells treated with oncogenic Ras, most likely because induction of senescence via this stimulus is less effective, as evaluated by means of the senescence marker, senescence-associated β-galactosidase (SA-β-gal) activity (Figure 1C) (Dimri et al., 1995). Given that Cdt1 switching per se does not infer that cells have entered into G1, we examined changes in the expression of various mitotic regulators as well as known senescence markers. All mitotic regulators tested were decreased and phosphorylation of histone H3 at serine 10 (H3-P-S10), a mitotic marker, was lost after exposure to senescence-inducing stimuli, and there was a marked increase in the population of tetraploid cells, suggesting that the cells had skipped mitosis before its initiation (see Figures S1A and S1B, available online). Although loss of mitotic regulators is a common feature of senescence, kinetics showing their loss prior to senescence induction indicated that this loss is a cause, but not a consequence, of senescence (Figure S1C). We then examined whether ectopic expression of the constitutively active form of cyclin B1-Cdk1 (cyclin B1-Cdk1AF fusion protein) or SV40 large T antigen in cells treated with IR resulted in entry of cells into mitosis or rereplication of DNA, respectively. In this case, one can expect that if cells are still in G2, then active cyclin B1-Cdk1 and SV40 large T antigen enforce the entry into mitosis but fail to initiate DNA rereplication, respectively. In contrast, if cells are in G1, then active cyclin B1-Cdk1 and SV40 large T antigen fail to force cells into mitosis but initiate DNA rereplication, respectively. We found that ectopic expression of cyclin B1-Cdk1AF fusion protein, which was used as a constitutively active form of cyclinB1-Cdk1 complex (Katsuno et al., 2009), enforced entry into mitosis in cells at 24 hr after treatment with IR, but not in cells at 48 hr (Figure S1D), by which time mitotic regulators had almost completely disappeared (completion of mitotic skipping) (Figure S1B). Expression of SV40 large T antigen resulted in DNA rereplication in cells at 48 hr after treatment, but not at 24 hr, generating an octaploid population (Figure S1E). Taken together, the results clearly indicated that a mitosis skip took place between 24 to 48 hr after IR treatment. Here, we considered that a mitotic skip had occurred when a cell exhibited both Cdt1 switching and loss of mitotic regulators without entry into mitosis. A similar cellular response was also observed in other HDFs, such as BJ and IMR90 cells, and in normal human retinal pigment epithelial cells (data not shown), indicating that this phenomenon is not cell type specific.

Senescent cells show very distinctive changes in morphology, such as assuming a flattened and enlarged shape. Although enlarged senescent cells were hardly detectable by FACScan until 36 hr after IR irradiation, they accumulated thereafter (Figure 1D). The vast majority of these large cells (F2) had a tetraploid DNA content, whereas many cells of normal size (F1) showed a diploid DNA content. These tetraploid cells were geminin negative and Cdt1 positive as well as SA-β-gal positive. Tetraploid fractions (G2) sorted by Hoechst intensities as G1 and G2 phase cells by FACScan at 3 and 7 days after DNA damage showed a marked increase in the expression of p16 and IL6, a senescence-associated cytokine, when compared with the diploid fraction (G1) (Figure 1E). In contrast, the expression of cyclin B1 was drastically decreased at 3 and 7 days specifically in G2 fractions. Furthermore, G2 fractions demonstrated a dramatic accumulation of p16 protein as well as SA-β-gal-positive cells at 7 days or later (Figures S1F and S1G); however, G1 fractions did not, even at 10 days after IR treatment. Taken together, cells in the tetraploid fraction predominantly appeared to undergo senescence.

Activation of p53 at G2 Is Necessary and Sufficient for Induction of Senescence

We then uncovered the molecular basis underlying mitotic skipping and determined whether it played a central role in senescence induction. p53 is known to be an essential factor for senescence induction (Rufini et al., 2013) and is activated in response to all senescence-inducing stimuli tested. p53 depletion markedly compromised Cdt1 switching and induced abnormal mitoses (Figure 2A). The number of cells that were SA-β-gal positive was reduced in p53-depleted cells (Figure 2B). Expression of mitotic regulators was almost completely lost in control senescent cells, whereas their expression was slightly induced in p53-depleted cells (Figure 2C).

When p53 was transiently expressed for 48 hr by the addition of doxycycline to cells synchronized at G2 by RO3306, time-lapse imaging revealed that Cdt1 switching occurred in 95% of cells, whereas cells synchronized at G1 or S phases were unaffected (Figure 2D). Levels of mitotic regulators in cells transiently expressing p53 at G2 were severely decreased, whereas those at G1 or S phases were readily detectable (Figure 2E). p16 was induced in cells transiently expressing p53 at G2 phase, but

(D) HCA2 cells at the indicated times after IR treatment (10 Gy) were stained with Hoechst 33342 and sorted by FSC and SSC as F1 and F2 and analyzed by FACScan.

(E) HCA2 cells at 0, 3, and 7 days after IR treatment (10 Gy) were stained with Hoechst 33342 and sorted by intensity as G1 and G2 phase cells by FACScan. The relative induction of p16, IL6, and cyc B1 transcripts were examined by qPCR analysis using the sorted fractions indicated as G1 and G2. Data are presented as means ±SD of at least three independent experiments. See also Figures S1A–S1G.

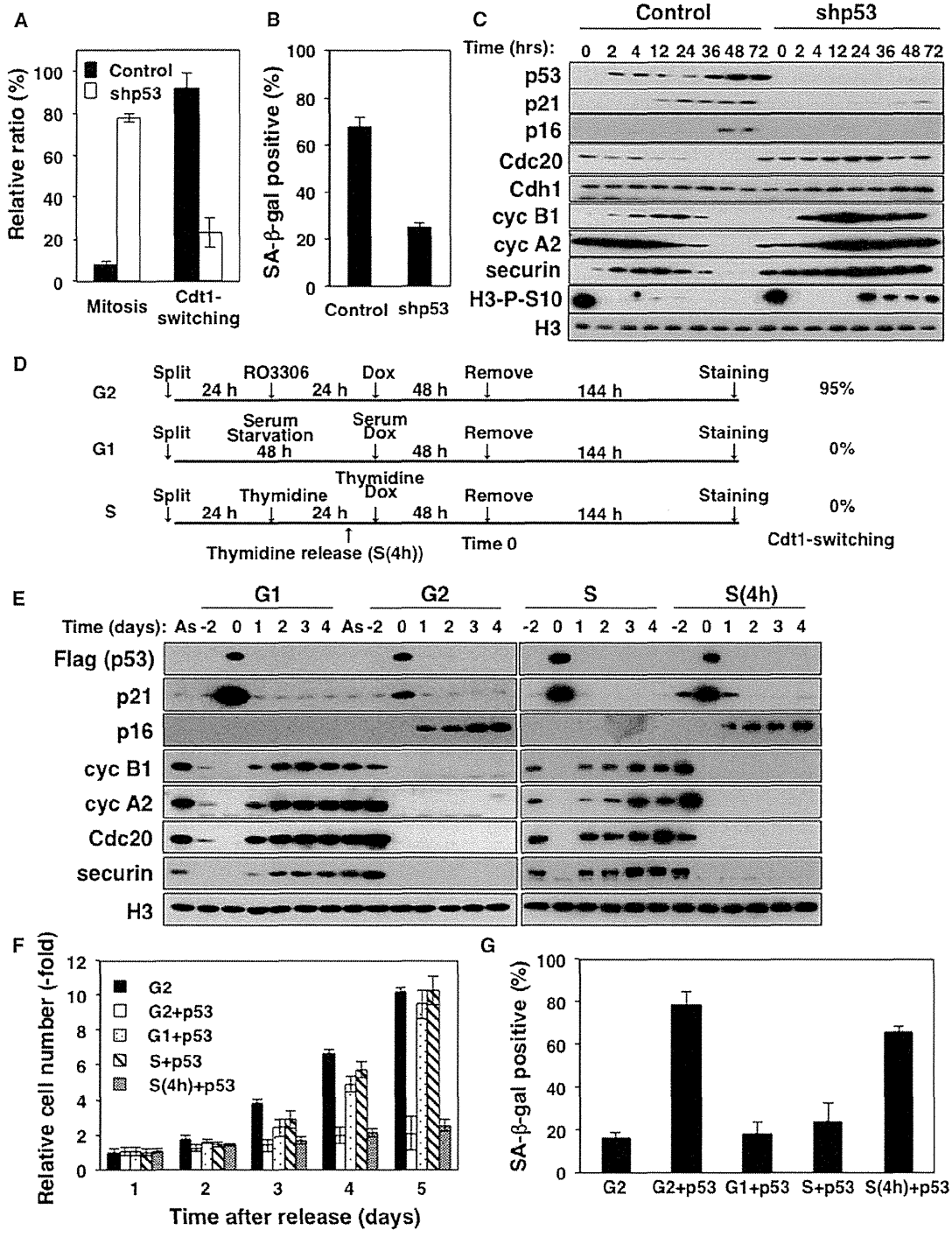

Figure 2. p53 Activation at G2 Phase Is Sufficient for the Induction of Senescence

(A and B) FUCCI-HCA2 cells expressing Tet-on sh-luciferase (control) or Tet-on sh-p53 (shp53) were treated with doxycycline (1 μg/ml). The treated cells were imaged by time-lapse microscopy after IR treatment (10 Gy). The relative ratio of Cdt1-switching cells was determined as in Figure 1B (A). The SA-β-gal-positive cells were identified as in Figure 1C (B). Data are presented as means ±SD of at least three independent experiments.

(C) Cell lysates of cells treated with sh-luciferase (control) or sh-p53 lentiviruses at the indicated time after IR treatment were subjected to immunoblotting using the indicated antibodies.

(D) Experimental outlines of cell-cycle-specific and transient expression of p53. Asynchronous FUCCI-HCA2 cells expressing Tet-on 3×Flag-p53 (As) were synchronized at G2, G1, or S phases by RO3306 (9 μM) for 24 hr, serum starvation for 48 hr, or thymidine (2 mM) for 24 hr, respectively. In some experiments, cells

(legend continued on next page)

not in those at G1 or S phases. p53 was only induced at day 0 in both cells. Intriguingly, cells transiently expressing p53 at G2 phase failed to proliferate, whereas those at G1 or S phase grew effectively (Figure 2F). The majority of cells transiently expressing p53 at G2 phase were SA-β-gal positive, whereas those at G1 or S phase were not (Figure 2G). Transient expression of p53 in cells released to G2 phase for 4 hr from a thymidine block resulted in loss of mitotic regulators, cessation of cell proliferation, and an increase in the SA-β-gal-positive fraction (Figures 2E–2G). Longer exposure of RO3306 per se did not induce Cdt1 switching, loss of mitotic regulators, and consequent induction of senescence (Figures S2A and 2B), although it might predispose cells to senescence upon p53 activation. These results clearly indicated that p53 activation at G2 was sufficient for senescence induction. Transient expression of p53 at G2 or G1 did not appear to induce DNA damage, eliminating the possibility that the mitosis skip and subsequent senescence induction by transient expression of p53 were not the result of a DDR (Figure S2C). Similar results were also observed in experiments using Nutlin 3a, a mdm2 inhibitor that activates endogenous p53 without causing DNA damage (Figure S2D). During the process of senescence induction in response to oxidative stress or oncogene activation, similar requirements for p53, p21, and Cdh1 in Cdt1 switching; its timing from S phase entry (please see below); loss of mitotic regulators; and senescence induction were observed when compared with IR-induced senescence (Figures S2E and S2F). The induction of senescence in p21-depleted cells appeared to be due to the fact that a majority of p21-depleted cells underwent cytokinesis failure, leading to eventual cell death within 6 days after treatment, and the remaining cells skipped mitosis, leading to senescence (see below). These results suggest that senescence induction in response to H_2O_2 or oncogenic Ras likely requires a p53-dependent mitosis skip.

Premature Activation of APC/C^{Cdh1} by the p53-p21 Axis Is Insufficient for a Mitosis Skip and Senescence Induction

p21 is a major downstream target of p53 (Levine and Oren, 2009). Time-lapse imaging revealed that upon DNA damage, many cells lacking p21 entered into mitosis but failed to complete cytokinesis and eventually died (Figures S3A and S3B). Transient expression of p21 at G2 phase failed to induce cessation of cell proliferation and senescence and strongly suppressed the expression of mitotic regulators, indicating that p21 induction is insufficient for senescence induction (Figures S3C–S3E).

p21 induction after various senescence-inducing stimuli resulted in premature activation of APC/C^{Cdh1}, showing a complex formation between Cdh1 and Cdc27 around 24 hr after treatment, indicating that it is a general feature of senescence induction (Takahashi et al., 2012) (Figure S3F). We then examined whether premature activation of APC/C^{Cdh1} by sequential inhibition of Cdk1 (RO3306) and Cdk2 (SU9516) was sufficient for the mitosis skip and subsequent senescence induction. Sequential inhibition of Cdk1 and Cdk2 resulted in Cdt1 switching, whereas inhibition of Cdk1 alone had no effect (Figure 3A, upper panel). Intriguingly, however, these Cdt1-positive cells rapidly entered into mitosis when the inhibitors were removed by washing (Figure S3G). These cells were not SA-β-gal positive, although treatment with Nutlin 3a at G2 effectively induced senescence (Figure 3A, lower panel). Mitotic regulators were still detectable after removal of the inhibitors, even in cells sequentially treated with Cdk1 and Cdk2 inhibitors or expressing p21, although significant reductions in the amounts of these proteins were observed (Figure 3B). These results suggested that premature activation of APC/C^{Cdh1} is insufficient for complete loss of mitotic regulators, indicating the existence of an alternative pathway(s) for suppressing the expression of mitotic regulators. Cdh1 depletion resulted in only a slight reduction in senescence induction (Figure 3C). It also resulted in an ultimate Cdt1 switching, presumably due to nonspecific degradation of geminin-fused fluorescence protein (Figure 3D). However, loss of Cdh1 markedly delayed the timing of Cdt1 switching, implicating its function in this process, because loss of Cdh1 did not affect S phase progression in the absence of DNA damage (Figure 3E). Thus, loss of mitotic regulators was still observed in cells lacking Cdh1 after DNA damage, although the timing of the disappearance of these proteins was markedly delayed (Figure 3F). Importantly, mitotic regulators were lost after DNA damage, even in the presence of the proteasome inhibitor MG132, although the effect of this reagent on the stabilization of mitotic regulators was significant at early time points (Figure 3G).

pRb Family Pocket Protein-Dependent Transcriptional Repression of Mitotic Regulators Is Required for a Mitosis Skip

Transcription of mitotic regulators was rapidly suppressed after treatment with Nutlin 3a (Figure 4A). This transcriptional repression was also observed in cells treated with H_2O_2 or expressing oncogenic Ras, indicating that this is also a general feature of senescence induction (Figure S4A). This suppression was completely dependent on the functional p53 but was only partly on the presence of p21 (Figure S4B). This transcriptional repression, as well as those of cyclin A2 and cyclin E1 (Figure S4C), was severely compromised when pRb, p107, and p130 were depleted (Figure 4B). Single or double depletion of the pocket proteins did not appear to affect the transcription of these genes (Figures S4D and S4E; data now shown). Thus, mitotic regulators were readily detectable, and their levels increased at later time points in cells lacking pRb, p107, and p130 when treated with IR (Figure 4C). Mitotic skipping was severely suppressed by

were released to G2 phase by removing thymidine 4 hr before addition of doxycycline (S(4h)). Cells were then treated with doxycycline (1 μg/ml) in the absence of RO3306 (G2), in the presence of 15% serum (G1) and thymidine (S), and released into fresh medium (Time 0). The relative ratios of Cdt1-switching cells were determined as in (**A**) and are shown in the figure.

(E and F) (E) Cell lysates of cells treated as in (D) at the indicated times were subjected to immunoblotting using the indicated antibodies. Time 0 is shown in (D). The relative number of cells treated as in (E) was determined as a multiple of those at day 1 (F). SA β-gal-positive cells were determined as in (B).

(G) Data are presented as means ±SD of at least three independent experiments. See also Figures S2A–S2F.

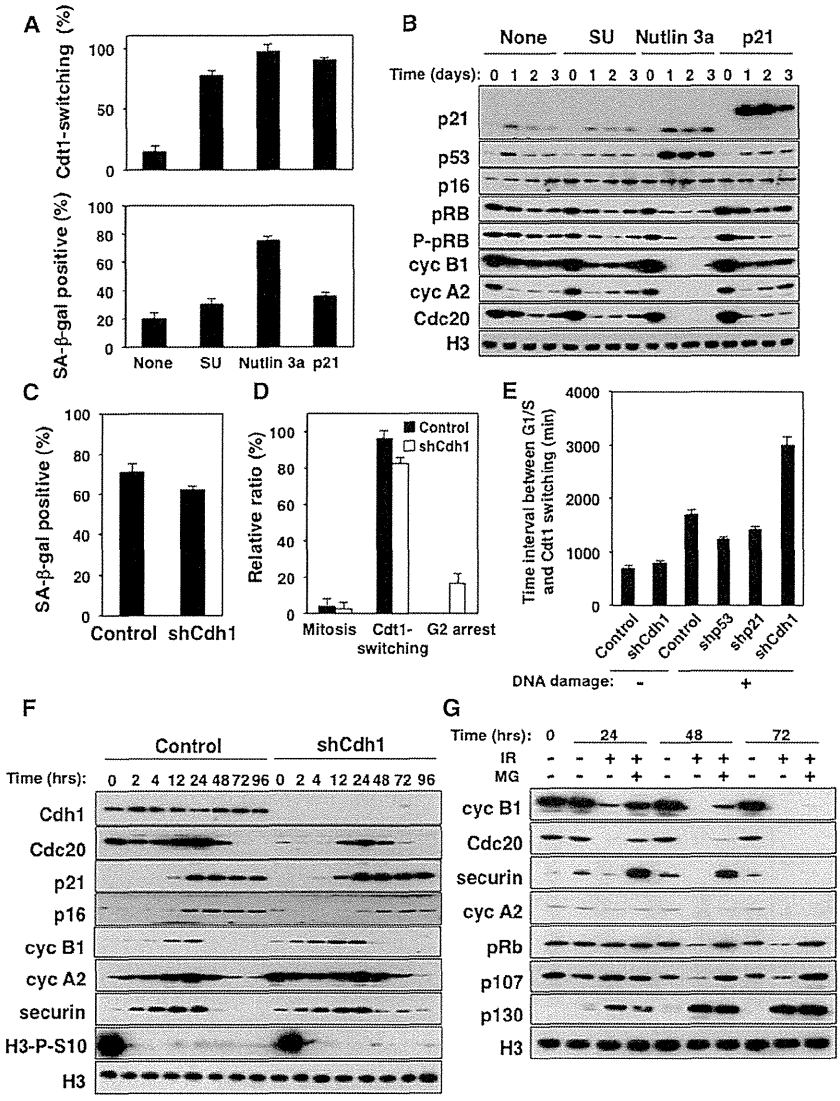

Figure 3. Induction of p21 at G2 Is Insufficient for Senescence Induction

(A) FUCCI-HCA2 cells expressing Tet-on 3×Flag p21 were synchronized at G2 by RO3306. The synchronized cells were untreated (None) or treated with SU9516 (SU; 10 μM), Nutlin 3a (5 μM), or doxycycline (1 μg/ml). The treated cells were then analyzed by time-lapse microscopy. The relative ratios of Cdt1-switching cells (upper panel) or SA-β-gal cells at 6 days after the treatments (bottom panel) were determined as in Figures 1B and 1C. Data are presented as means ±SD of at least three independent experiments.

(B) Cell lysates of cells treated as in (A) at the indicated times were subjected to immunoblotting analyses. Time 0 represents the day on which cells were treated.

(C and D) FUCCI-HCA2 cells expressing Tet-on sh-luciferase (control) or Tet-on sh-Cdh1 (shCdh1) were treated with doxycycline (1 μg/ml). Cells were then treated with IR (10 Gy) and subjected to SA-β-gal staining as in Figure 1C (C) or time-lapse microscopy for determining the relative ratio of Cdt1-switching cells as in Figure 1B (D). Data are presented as means ±SD of at least three independent experiments.

(E) Time intervals for cells treated as in (C) between G_1/S (change from red to green color) and Cdt1 switching (change from green to red color) with or without DNA damage were determined by examining at least 100 cells.

(F) Cell lysates from (C) at the indicated times after IR were subjected to immunoblotting using the indicated antibodies.

(G) Cell lysates from HCA2 cells treated with or without IR (10 Gy) at the indicated times in the presence or absence of MG132 (MG; 10 μg/ml) were subjected to immunoblotting using the indicated antibodies. See also Figures S3A–S3G.

triple knockdown of pRb family pocket genes, although the appearance of Cdt1 switching cells was apparently unaffected (Figure 4D). Senescence induction in cells lacking all three pRb family proteins could not be analyzed, because these cells were not healthy in the presence of DNA damage after 6 days of culture (Figure 4E).

Loss of p16 did not appear to affect mitosis skip (Figures 5A and 5B). However, consistent with a previous report (Beauséjour et al., 2003), conditional knockdown of p16 by addition of doxycycline to cells treated with Nutlin 3a at G2 phase (Figure 5C) caused the reversal of the senescent state and allowed entry into S phase (Figure 5D), cell proliferation (Figure 5E), and re-expression of mitotic regulators (Figure S5). Interestingly, fluorescence-activated cell sorting (FACS) analysis revealed the appearance of octaploid cells after depletion of p16, further supporting the idea that senescent cells are tetraploid G1 cells (Figure 5F). Taken together, the present results suggest a general mechanism of senescence induction (Figure 5G). Activation of p53 at G2 in response to senescence-inducing stimuli leads to induction of p21 that suppresses both Cdk1 and Cdk2 activities. This suppression results in the premature activation of APC/C^{Cdh1} that degrades various mitotic regulators, leading to the Cdt1 switching. Activated p53 also enhances functions of pRb family pocket proteins through unknown mechanisms other than p21-dependent suppression of Cdk activities (Figure S4B) and consequently suppresses transcription of mitotic regulators. Both pathways cooperatively ensure mitosis skipping, leading to senescence induction.

Transient Expression of Cdh1-4A and pRb7LP at G2 Is Sufficient for Senescence Induction

In order to confirm our above model of senescence induction, we first examined whether transient expression at G2 of a constitutively active pRb (pRb7LP), in which all Cdk phosphorylation sites were substituted (Angus et al., 2003), would be sufficient for senescence induction under premature activation of APC/C^{Cdh1}. Transient expression (24 hr) of pRb7LP by the addition of

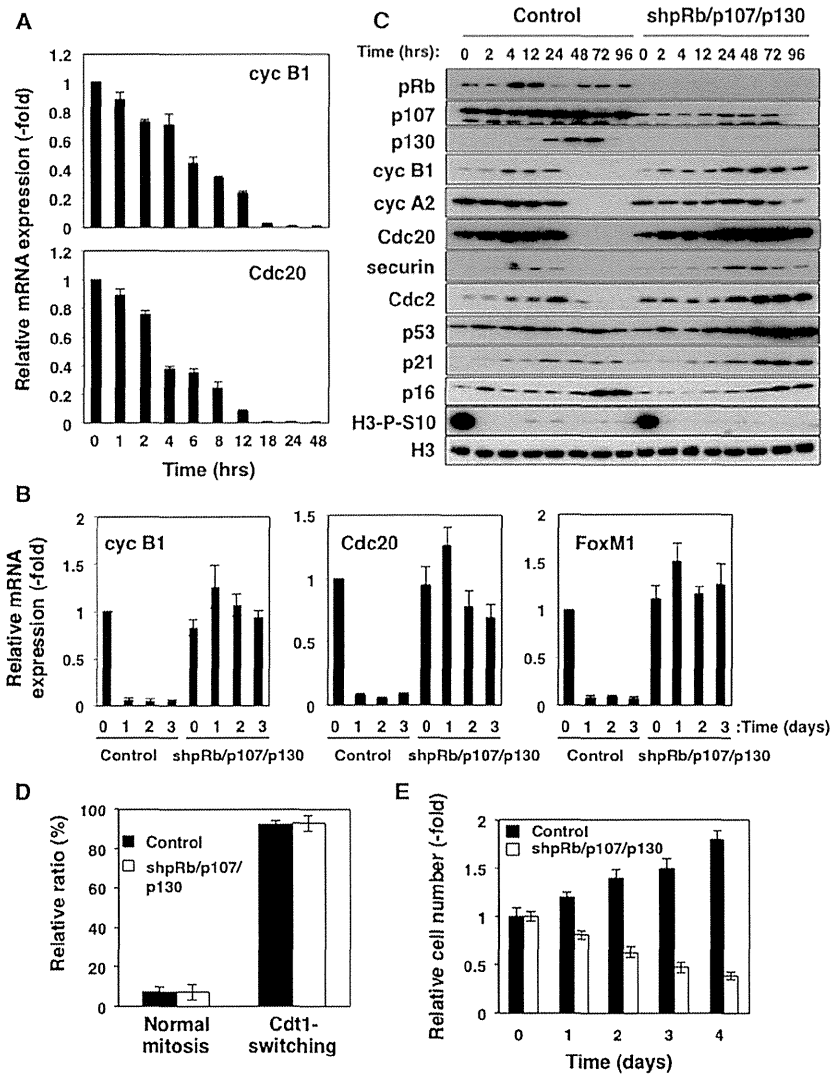

Figure 4. pRb Family Proteins Are Essential for Transcriptional Repression of Mitotic Regulators

(A and B) The relative expression of the indicated transcripts were determined by qPCR analysis using total RNA from HCA2 cells at the indicated times after Nutlin 3a (A) or HCA2 cells expressing Tet-on sh-luciferase (control) or Tet-on sh-pRb, sh-p107, and sh-p130 (shpRb/p107/p130) in the presence of doxycycline (1 μg/ml) at the indicated times after IR treatment (10 Gy) (B). The results are presented as a multiple of those without treatment. Data are presented as means ±SD of at least three independent experiments.

(C–E) (C) Cell lysates from (B) at the indicated times after IR treatment were subjected to immunoblotting using the indicated antibodies. FUCCI-HCA2 cells expressing Tet-on sh-luciferase (control) or Tet-on sh-pRb, sh-p107, and sh-p130 (shpRb/p107/p130) were treated with doxycycline (1 μg/ml) for 24 hr. The treated cells were subjected to time-lapse microscopy after IR treatment (10 Gy). The relative ratio of Cdt1-switching cells was determined as in Figure 1B (D). The relative cell number was determined and expressed as a multiple of those without treatment (E). Data are presented as means ±SD of at least three independent experiments. See also Figures S4A–S4E.

doxycycline to G2 cells, in the presence of a Cdk2 inhibitor to prematurely activate Cdh1 (Figure 6A), resulted in impaired cell proliferation (Figure 6B) and an increase in the population of cells staining positive for SA-β gal (Figure 6C). The expression of mitotic regulators was also greatly decreased in these cells (Figure 6D). Under these conditions, treatment with a Cdk2 inhibitor did not affect the transcriptional suppression of mitotic regulators, although it markedly enhanced loss of mitotic regulators (Figures S6A and S6B). Transient expression (24 hr) of pRb7LP at G2 in the absence of a Cdk2 inhibitor was far less effective in inducing senescence than when the inhibitor was present, suggesting a role for prematurely activated Cdh1 in mitosis skip (Figure S6C). However, longer expression (72 hr) of pRb7LP at G2 ultimately induced senescence, supporting the dispensability of Cdh1 for senescence induction (Figures 3C–3F).

We therefore asked whether transient expression (24 hr) of both a constitutively active mutant of Cdh1 (Cdh1-4A) (Lukas et al., 1999) and pRb7LP is sufficient for a mitosis skip and senescence induction. When both proteins were transiently expressed in synchronized G2 cells (Figure 6E), cessation of cell proliferation (Figure 6F), an increase in the population of SA-β-gal-positive cells (Figure 6G), and a loss of mitotic regulators were observed (Figure 6H), whereas expression of either one alone failed to have the same effect. Expression of both proteins in asynchronous cells also failed to induce senescence, further confirming that a mitosis skip is necessary and sufficient for the induction of cellular senescence. The resulting senescence phenotype of the cells was further confirmed by the induction of p16 and senescence-associated cytokines such as IL-6 and IL-8 (Figure S6D). Transient expression of both proteins did not induce DNA damage, eliminating the possibility that senescence induction was an indirect consequence of an activated DDR (Figure S6E).

Role of the Mitosis Skip in the Induction of Senescence In Vivo

Finally, we asked whether mitotic skipping plays a role in in vivo senescence. Human nevi are benign tumors of melanocytes with frequent mutations in BRAF, a protein kinase and downstream effector of Ras, and were reported to be invariably positive for SA-β-gal staining, suggesting that nevus cells are oncogene-induced senescent cells in vivo (Michaloglou et al., 2005). Therefore, we examined whether human nevus cells were tetraploid

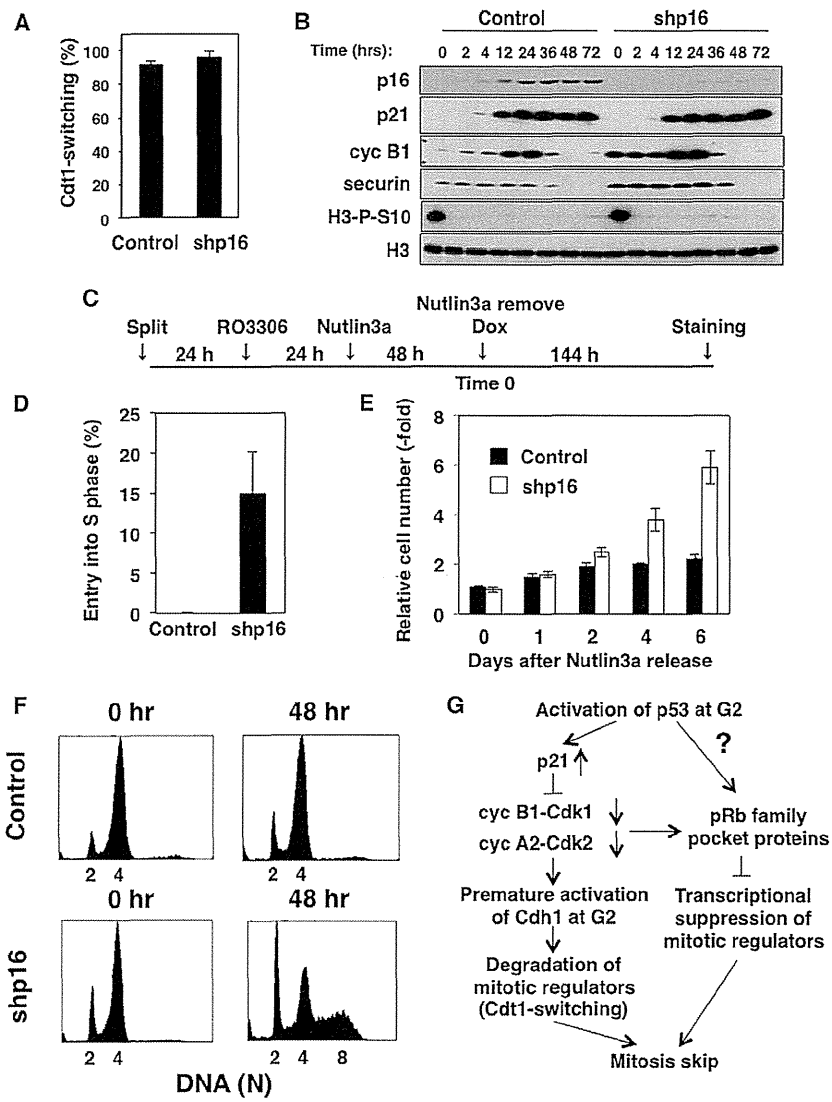

Figure 5. p16 Is Essential for the Maintenance, but Not for the Induction of Cellular Senescence

(A) FUCCI-HCA2 cells expressing Tet-on sh-luciferase (control) or Tet-on sh-p16 in the presence of doxycycline (1 μg/ml) for 24 hr were subjected to time-lapse microscopy after IR treatment (10 Gy). The relative ratio of Cdt1-switching cells was determined as in Figure 1B. Data are presented as means ±SD of at least three independent experiments.

(B) Cell lysates from HCA2 cells treated as in (A) at the indicated times after IR treatment were subjected to immunoblotting using the indicated antibodies.

(C–E) (C) The experimental outline of p16 depletion after the induction of cellular senescence. FUCCI-HCA2 cells treated as in (A) were synchronized at G2 phase by RO3306 (9 μM), treated with Nutlin 3a (5 μM), and released into fresh medium in the presence of doxycycline (1 μg/ml) (Time 0). FUCCI-HCA2 cells treated as in (C) were subjected to time-lapse microscopy. The relative ratio of geminin-switching cells (entry into S phase) was determined (D). The relative cell number at the indicated times was determined from cells treated as in (C). The results are shown as a multiple of those at time 0 (E). Data are presented as means ±SD of at least three independent experiments.

(F) Cells treated as in (C) at the indicated times were analyzed by FACScan.

(G) Schematical model of molecular pathways that induce a mitosis skip in response to senescence-inducing stimuli. See also Figure S5.

G1 cells generated as a result of a mitosis skip in vivo. Pathological sections of human nevi from three distinct individuals were subjected to DAPI staining to measure the DNA content of each cell. In order to normalize the staining efficiencies, these sections were also counterstained with anti-histone H3 antibodies (Figure 7A). Very intriguingly, nevus cells from all three individuals possessed almost twice the DNA content of control epidermis and endothelium cells (Figure 7B). Similar results were also obtained when sections were counterstained with anti-TBP antibodies (Figure S7). Immunohistochemical analysis revealed that nevi were both Ki-67 and cyclin B1 negative, whereas many hair follicle cells are Ki-67 positive and some sweat gland cells are cyclin B1 positive (Figure 7C). Taken together, these results suggested that human nevus cells are arrested in G1 phase with a tetraploid DNA content, which would likely be consistent with the role of the mitosis skip in in vivo senescence.

DISCUSSION

One-way progression of the cell cycle is governed by two distinct levels of regulation; one is transcriptional control of genes (Giacinti and Giordano, 2006), and the other is degradation of proteins involved in chromosomal DNA replication and segregation (Vodermaier, 2004). Therefore, cell-cycle phases, particularly G1 and G2, could be defined not by the content of genomic DNA alone, but by the status of the above two systems. In the present study, time-lapse live-cell imaging revealed that senescent cells induced by all stimuli tested skipped mitosis before growth arrest in various types of human cells (Figures 1A–1C and S1A–S1E). Mitotic skipping was evidenced by the fact that senescent cells exhibited an accumulation of a Cdt1-fused fluorescent marker without entry into mitosis, had a tetraploid DNA content, and lacked mitotic regulators. Importantly, this skipping was further confirmed by observations that after a mitosis skip, cells did not enter into mitosis by the expression of an active form of cyclin B1-Cdk1 fusion protein and rereplicate DNA by the expression of SV40 large T antigen, generating an octaploid population (Figures S1D and S1E). Consistent with this, a marked increase in the population of tetraploid cells was reported after senescent stimuli, such as DNA damage and

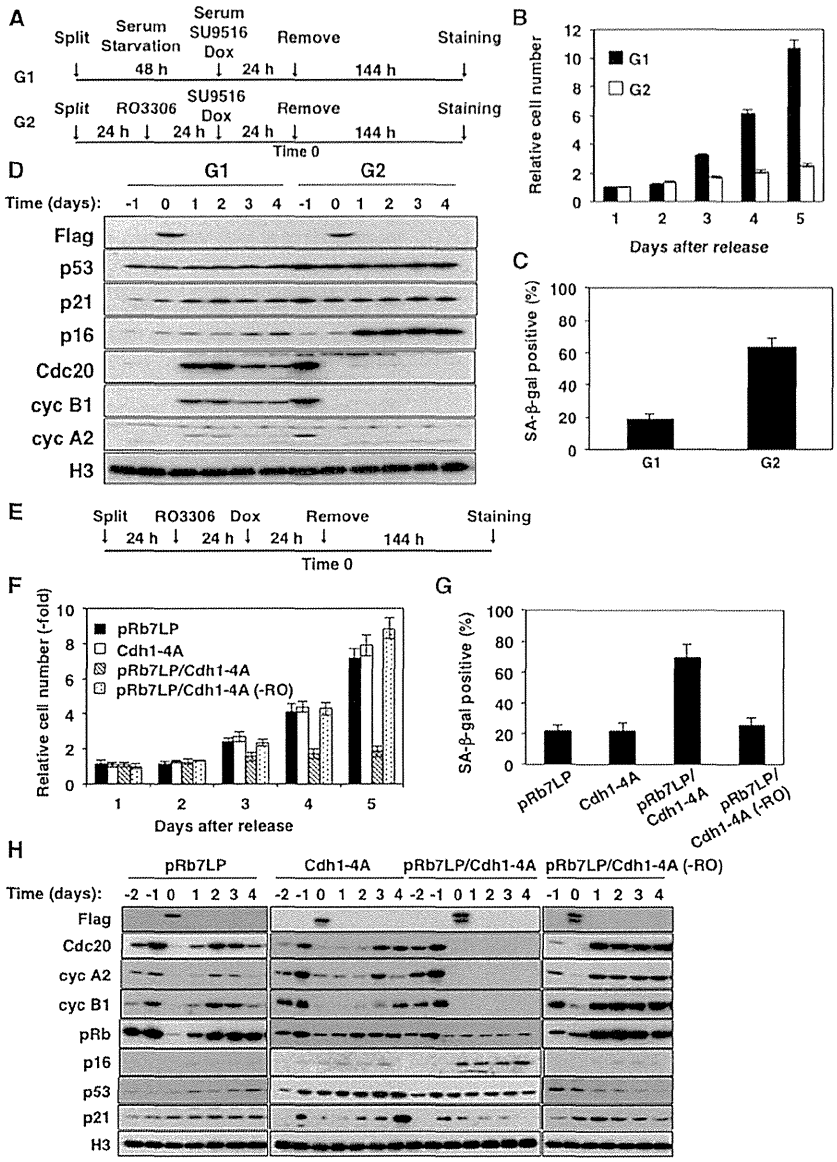

Figure 6. Expression of pRb7LP and Cdh1-4A at G2 Is Sufficient for the Induction of Senescence

(A–C) (A) The experimental outline of the cell-cycle-specific and transient expression of Tet-on 3×Flag-pRb7LP. HCA2 cells expressing Tet-on 3×Flag-pRb7LP were synchronized at G0 or G2 by serum starvation or RO3306 (9 μM), respectively. The synchronized cells were treated with SU9516 (10 μM) and doxycycline (1 μg/ml) and then released into fresh medium (Time 0). The relative cell number of cells treated as in (A) was determined (B). The relative ratio of SA-β-gal-positive cells treated as in (A) was determined as in Figure 1C (C). Data are presented as means ±SD of at least three independent experiments.

(D) Cell lysates treated as in (A) were subjected to immunoblotting using the indicated antibodies.

(E) The experimental outline of the transient expression of Tet-on 3×Flag-pRb7LP and Tet-on 3×Flag-Cdh1-4A at G2. HCA2 cells expressing Tet-on 3×Flag-pRb7LP *and/or* 3×Flag-Cdh1-4A were synchronized at G2 with RO3306 (9 μM), treated with doxycycline (1 μg/ml), and then released into fresh medium (Time 0). The relative number of cells treated as in (E) was determined (F). −RO; without RO3306 treatment. The relative ratio of SA-β-gal-positive cells treated as in (E) was determined as in (C).

(G) Data are presented as means ±SD of at least three independent experiments.

(H) Cell lysates from cells treated as in (E) were subjected to immunoblotting using the indicated antibodies. −RO; without RO3306 treatment. See also Figures S6A–S6E.

telomere shortening (Mao et al., 2012; Ye et al., 2013). Senescent mitotic skipping is a form of cell-cycle arrest that is distinct from mitotic slippage or a postmitotic checkpoint that results from incomplete mitosis or impaired cytokinesis, because the latter form is induced after entry into mitosis (Andreassen et al., 2001; Lanni and Jacks, 1998). In addition, it should be noted that mammalian cells were reported not to possess checkpoints for tetraploidy or an aberrant centrosome number (Uetake and Sluder, 2004; Wong and Stearns, 2005).

Many signals and genes are reported to be involved in the induction of senescence, depending on the experimental context, demonstrating the complex nature of the phenotype (Campisi and d'Adda di Fagagna, 2007; Courtois-Cox et al., 2008). However, all senescent signals ultimately lead to p53 and pRb family pocket proteins, both of which are essential for senescence induction (Dannenberg et al., 2000; Rufini et al., 2013; Sage et al., 2000). Although it is widely believed that the mere activation of pRb and p53 is not sufficient to trigger senescence, we found that transient activation of p53, specifically at G2, was enough to trigger senescence through induction of a mitosis skip (Figures 2D–2G). This signal transcriptionally induces p21, which in turn inhibits cyclin B1/Cdk1 and prematurely activates APC/C^{cdh1} (Figure S3F) (Baus et al., 2003; Wiebusch and Hagemeier, 2010; Takahashi et al., 2012). p21 was also shown to function in the regulation of Cdk2 activity at normal mitosis, making the proliferation-quiescence decision (Spencer et al., 2013). Therefore, the level of p21 at mitosis might be a key determining factor to decide whether cells undergo senescence, quiescence, or proliferation.

Upon persistent telomere damage, a distinct form of mitosis skip in p53-deficient cells was also reported to generate polyploidy by premature activation of APC/C^{cdh1}, the key result of Chk1-dependent suppression of Cdk1 (Davoli et al., 2010). However, activation of APC/C^{cdh1} at G2 was insufficient for a mitosis skip during senescent induction (Figures 3A and 3B). Deprotected telomeres that remain in a fusion-resistant intermediate

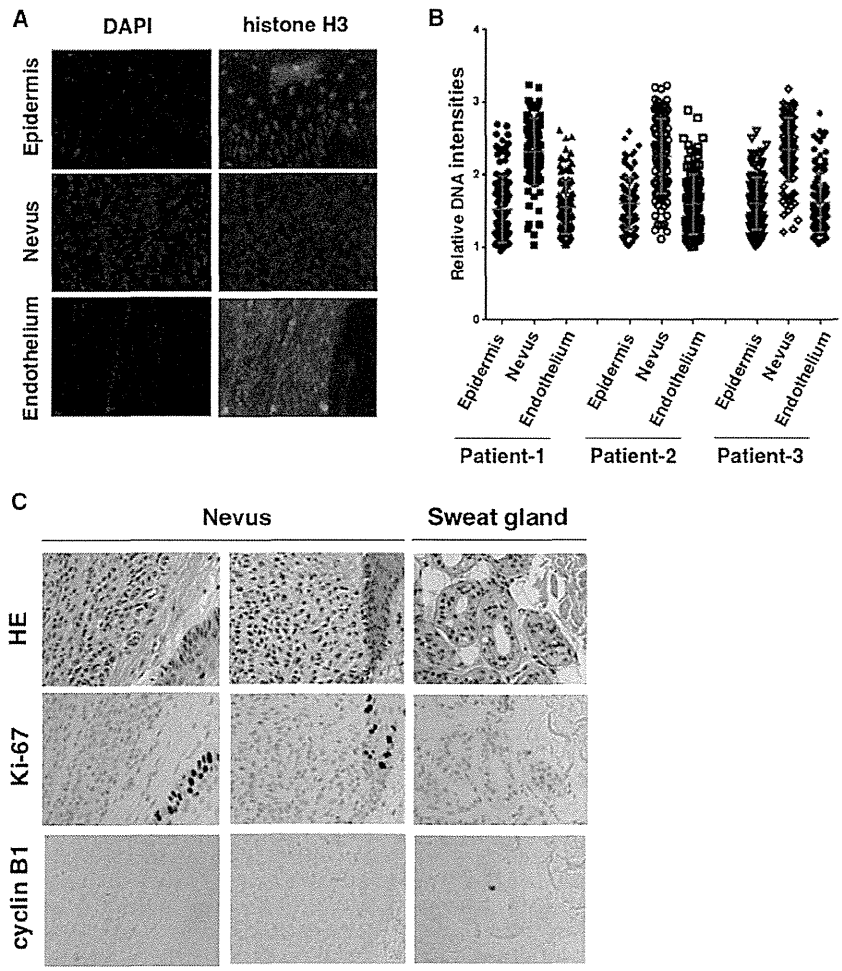

Figure 7. Human Melanocytic Nevus Cells Are Ki-67 and Cyclin B1 Negative, but Possess Almost Twice the DNA Content of Control Cells

(A) Paraffin-embedded sections of human nevi were subjected to immunohistochemical staining with anti-histone H3 antibody (green) along with DAPI staining for DNA (blue). The representative images for epidermis, nevus, and endothelium are shown.

(B) Fluorescence intensities of DAPI and anti-histone H3 signals in (A) were quantified with Image J software. The quantified DAPI intensity of each cell was normalized by the corresponding anti-histone H3 intensity, and the results are shown as relative DNA intensities. Nevi, epidermis, and endothelia from three patients were analyzed. Data are averages ±SD (n = 100).

(C) Paraffin-embedded sections of human nevi and sweat gland were subjected to hematoxylin and eosin staining (HE) and immunohistochemical staining using anti-Ki-67 antibody (brown) or anti-cyclin B1 antibody (green). See also Figure S7.

state were also shown to trigger a cell-cycle exit from G1. This intermediate telomere erosion activates unique DDRs that fail to activate G2/M checkpoint, leading to a p53-dependent G1 arrest (Cesare et al., 2013). However, actual involvement of this cell-cycle exit in senescence induction is unclear, because Chk1- and Chk2-dependent G2/M checkpoint activation is evident in telomere-initiated senescence (d'Adda di Fagagna et al., 2003).

The most striking observation in the present study was senescence induction by transient expression of both Cdh1-4A and pRb7LP in cells at G2, but not at other phases of the cell cycle (Figures 6E–6H). Although the unique and nonredundant role of pRb in the transcriptional repression of a certain set of E2F target genes during senescence was reported (Chicas et al., 2010), a single or double depletion of pRb family pocket proteins did not appear affect the mitosis skip and senescence induction (Figures S4D and S4E; data not shown), indicating that their function is at least in part redundant. E2F7 is a p53 target and has been proposed to compensate for the loss of pRb in repressing mitotic regulators (Aksoy et al., 2012). However, under our experimental conditions, the presence of E2F7 was not sufficient for suppressing the expression of mitotic regulators in the absence of all pRb family pocket proteins (Figure 4C), although our results do not exclude the possibility that it plays a role in the maintenance of senescence. Another surprising observation was the dispensable role of p16 in mitotic skipping and senescence induction (Figures 5A and 5B), although it has been reported to be essential for the maintenance of senescence (Figures 5D–5F) (Beauséjour et al., 2003). It should be noted that induction of p16 consistently appeared to be a later event than that of p53 and p21 (Figure 2C). Intriguingly, a loss of p16 in senescent cells caused reentry into S phase, resulting in an increased octaploid population.

Accumulating evidence has suggested that senescence plays a pivotal role in antitumorigenesis and aging-related changes in vivo (Campisi and d'Adda di Fagagna, 2007; Halazonetis et al., 2008). For example, human melanocytic nevi with BRAF mutations show typical hallmarks of senescence, suggesting that oncogene-induced senescence is a bona fide physiological process (Michaloglou et al., 2005). Importantly, nevus cells were Ki-67 negative and cyclin B1 negative but possessed almost twice the DNA content of control cells, suggesting that oncogene-induced senescent cells are tetraploid G1 cells in vivo (Figures 7A–7C and S7). Therefore, these results are consistent with in vitro observations that the mitosis skip plays a necessary and sufficient role in the induction of senescence.

EXPERIMENTAL PROCEDURES

Plasmid Construction

To generate lentivirus-based shRNA constructs, a 19–21 base shRNA-coding fragment with a 5′-ACGTGTGCTGTCCGT-3′ loop was introduced into

pENTR4-H1 digested with *AgeI*/EcoRI. To insert the H1tetOx1-shRNA into a lentivirus vector, we mixed the resulting pENTR4-H1-shRNA vector and CS-RfA-ETBsd, CS-RfA-ETHygro, or CS-RfA-ETPuro vector with Gateway LR clonase (Invitrogen). All the target sequences for lentivirus-based sh-RNAs are summarized in Table S1.

To construct Tet-on inducible lentivirus constructs, the *BamHI/ NotI* fragment PCR containing cDNA for human p16, p21, p53, pRb7LP (Angus et al., 2003), Cdh1-4A (Lukas et al., 1999), or H-RAS^{val12} (Barradas et al., 2009) was inserted into a pENTR-1A vector (Invitrogen) containing 3×Flag epitope digested with *BamHI/NotI*. The resultant plasmid was mixed with CS-IV-TRE-RfA-UbC-Puro vector, or CS-IV-TRE-RfA-UbC-Hygro vector, and reacted with Gateway LR clonase to generate the lentivirus plasmid.

Immunoblotting Analyses

Immunoblotting was performed as previously described (Katsuno et al., 2009). All antibodies used in this study are listed in Table S2.

Cell Culture

Early passage normal HDFs, HCA2 (Nakanishi et al., 1995), BJ (ATCC), IMR90 (ATCC), IMR90-ER:RAS ^{val12} (Barradas et al., 2009), and HEK293T cells (ATCC) were cultured in Dulbecco's modified Eagle's medium (DMEM) supplemented with 10% fetal bovine serum (FBS). For the serum starvation experiment, cells were cultured with DMEM supplemented with 0.5% FBS for 48 hr. Cells were synchronized at early S phase by treatment with 2 mM of thymidine (Sigma-Aldrich) for 24 hr or at G2 phase by treatment with 9 μM of RO3306 (Roche) for 24 hr. Nutlin-3a (Sigma-Aldrich), SU9516 (Merck4 Biosciences), MG132 (Sigma-Aldrich), or NU7026 (Sigma-Aldrich) was used at a concentration of 5 μM, 10 μM, 10 μg/ml, or 10 μM, respectively, for the indicated interval. Treatments with IR at 10 Gy, Etoposide (Sigma-Aldrich) at 200 nM for 24 hr and H_2O_2 (Sigma-Aldrich) at 50 μM for 24 hr were used to generate IR-induced, DNA damage-induced, and oxidative stress-induced senescent cells, respectively. Senescent cells treated with IR at the 10 Gy dose were analyzed 6 days after treatment and were evaluated by SA-β-gal staining. Oncogene-induced senescent cells were generated by the expression of ER-H-Ras^{val12} or 3×Flag-H-Ras^{val12} in the presence of 4-OHT for 8 days. Replicative senescent cells were generated by the culture of near senescent HDFs (PD > 60).

Virus Generation and Infection

Lentiviruses expressing the respective shRNAs or genes were generated by cotransfection of 293T cells with pCMV-VSV-G-RSV-Rev, pCAG-HIVgp, and the respective CS-RfA-ETBsd, CS-RfA-ETHygro, CS-RfA-ETPuro, CS-IV-TRE-RfA-UbC-Puro, or CS-IV-TRE-RfA-UbC-Hygro using the calcium phosphate coprecipitation method. Cells infected with the indicated viruses were treated with 10 μg/ml of blasticidin (Invitrogen), 200 ng/ml of hygromycin (Sigma-Aldrich), and/or 2 μg/ml of puromycin (Sigma-Aldrich) for 2–3 days. Doxycycline (Sigma-Aldrich) was added to the medium at a concentration of 1 μg/ml for inducible expression of the respective shRNAs or genes.

Time Lapse Microscopy

HCA2 or IMR90-ER:RAS^{val12} cells expressing FUCCI 2.1 indicators (pMXs-AmCyan-hGeminin [1/110] and pMXs-IP-mCherry-hCdt1 [30/120]) were cultured on a glass-based dish (Iwaki), placed on the stage of a BZ-9000 (Keyence) equipped with an environmental chamber (Keyence), providing an adequate temperature, humidity, and CO_2 control. Time-lapse images were captured every 20 min for 72 hr with a set of green 494/20 and 536/40 emission filters. Images were analyzed using BZ-9000 software.

SA-β-Gal Staining

SA-β-gal staining was performed as previously described (Dimri et al., 1995).

Quantitative RT-PCR

Total RNA was extracted using ISOGEN II (Wako) according to the manufacturer's instructions. For quantitative RT-PCR analysis, cDNAs were synthesized using a SuperScript II cDNA synthesis kit (Invitrogen). Real-time PCR amplifications were performed in 96-well optical reaction plates with Power SYBR Green PCR Master Mix (Applied Biosystems). The relative expression values of each gene were determined by normalization to GAPDH expression for each sample. Primer sequences are available upon request.

FACS Analysis and FACS Sorting

Cell-cycle profiles were analyzed by a standard procedure using a FACS CANT2 (BD Biosciences). Diploid and tetraploid fractions were isolated by FACS sorting using a BD FACSAria-2 cell sorter (BD Biosciences) after incubation with 10 μM Hoechst 33342 (Wako) for 10 min.

Immunohistochemistry

Human pathological sections containing nevi were fixed in 4% formaldehyde overnight and embedded in paraffin. Paraffin sections were deparaffinized, rehydrated, and incubated with peroxidase blocking reagent (DAKO). The tissue was incubated with the primary antibodies 96C10 for histone H3 (Cell Signaling), MIB-1 for Ki-67 (DAKO), and GNS1 for cyclin B1 (Santa Cruz). Primary antibody binding was detected using a FITC-linked secondary antibody or a HRP-linked antibody and revealed by conventional immunostaining using DAB (DAKO) or HistoGreen (ABC Scientific) as a substrate. This study was approved by the Ethics Committee of Nagoya City University Graduate School of Medical Sciences, Nagoya, Japan. All subjects provided written informed consent.

SUPPLEMENTAL INFORMATION

Supplemental Information includes seven figures, two tables, and Supplemental Experimental Procedures and can be found with this article online at http://dx.doi.org/10.1016/j.molcel.2014.05.003.

ACKNOWLEDGMENTS

We are grateful to Dr. Atsushi Miyawaki and Dr. Asako Sakaue-Sawano for providing a *FUCCI* system; Dr. Olivia-Pereira Smith, Dr. Keiko Kono, and Dr. Atsuya Nishiyama for critical reading of the manuscript; and Dr. Gordon Peters, Dr. Masashi Narita, Dr. Jiri Lucas, Dr. Julien Sage, Dr. Claus Storgaard Sorensen, Dr. Oscar Fernandez-Capetillo, Dr. Krinstin Helin, Dr. Kaoru Tominaga, and Dr. Takahisa Hirokawa for reagents and suggestions. We are also indebted to Dr. Chisato Yamada-Namikawa and the other members of Dr. Nakanishi's laboratory for technical assistance. M.N. was supported by a Grant-in-Aid for Scientific Research on Innovative Area "Cell fate control," Scientific Research (A), and Challenging Exploratory Research from MEXT Japan.

Received: December 9, 2013
Revised: March 6, 2014
Accepted: April 18, 2014
Published: June 5, 2014

REFERENCES

Adams, P.D. (2009). Healing and hurting: molecular mechanisms, functions, and pathologies of cellular senescence. Mol. Cell *36*, 2–14.

Aksoy, O., Chicas, A., Zeng, T., Zhao, Z., McCurrach, M., Wang, X., and Lowe, S.W. (2012). The atypical E2F family member E2F7 couples the p53 and RB pathways during cellular senescence. Genes Dev. *26*, 1546–1557.

Andreassen, P.R., Lohez, O.D., Lacroix, F.B., and Margolis, R.L. (2001). Tetraploid state induces p53-dependent arrest of nontransformed mammalian cells in G1. Mol. Biol. Cell *12*, 1315–1328.

Angus, S.P., Solomon, D.A., Kuschel, L., Hennigan, R.F., and Knudsen, E.S. (2003). Retinoblastoma tumor suppressor: analyses of dynamic behavior in living cells reveal multiple modes of regulation. Mol. Cell. Biol. *23*, 8172–8188.

Barradas, M., Anderton, E., Acosta, J.C., Li, S., Banito, A., Rodriguez-Niedenführ, M., Maertens, G., Banck, M., Zhou, M.M., Walsh, M.J., et al. (2009). Histone demethylase JMJD3 contributes to epigenetic control of INK4a/ARF by oncogenic RAS. Genes Dev. *23*, 1177–1182.

Baus, F., Gire, V., Fisher, D., Piette, J., and Dulić, V. (2003). Permanent cell cycle exit in G2 phase after DNA damage in normal human fibroblasts. EMBO J. *22*, 3992–4002.

Beauséjour, C.M., Krtolica, A., Galimi, F., Narita, M., Lowe, S.W., Yaswen, P., and Campisi, J. (2003). Reversal of human cellular senescence: roles of the p53 and p16 pathways. EMBO J. *22*, 4212–4222.

Burkhart, D.L., and Sage, J. (2008). Cellular mechanisms of tumour suppression by the retinoblastoma gene. Nat. Rev. Cancer *8*, 671–682.

Campisi, J., and d'Adda di Fagagna, F. (2007). Cellular senescence: when bad things happen to good cells. Nat. Rev. Mol. Cell Biol. *8*, 729–740.

Cesare, A.J., Hayashi, M.T., Crabbe, L., and Karlseder, J. (2013). The telomere deprotection response is functionally distinct from the genomic DNA damage response. Mol. Cell *51*, 141–155.

Chicas, A., Wang, X., Zhang, C., McCurrach, M., Zhao, Z., Mert, O., Dickins, R.A., Narita, M., Zhang, M., and Lowe, S.W. (2010). Dissecting the unique role of the retinoblastoma tumor suppressor during cellular senescence. Cancer Cell *17*, 376–387.

Cobrinik, D. (2005). Pocket proteins and cell cycle control. Oncogene *24*, 2796–2809.

Courtois-Cox, S., Jones, S.L., and Cichowski, K. (2008). Many roads lead to oncogene-induced senescence. Oncogene *27*, 2801–2809.

d'Adda di Fagagna, F., Reaper, P.M., Clay-Farrace, L., Fiegler, H., Carr, P., Von Zglinicki, T., Saretzki, G., Carter, N.P., and Jackson, S.P. (2003). A DNA damage checkpoint response in telomere-initiated senescence. Nature *426*, 194–198.

Dannenberg, J.H., van Rossum, A., Schuijff, L., and te Riele, H. (2000). Ablation of the retinoblastoma gene family deregulates G(1) control causing immortalization and increased cell turnover under growth-restricting conditions. Genes Dev. *14*, 3051–3064.

Davoli, T., Denchi, E.L., and de Lange, T. (2010). Persistent telomere damage induces bypass of mitosis and tetraploidy. Cell *141*, 81–93.

Dimri, G.P., Lee, X., Basile, G., Acosta, M., Scott, G., Roskelley, C., Medrano, E.E., Linskens, M., Rubelj, I., Pereira-Smith, O., et al. (1995). A biomarker that identifies senescent human cells in culture and in aging skin in vivo. Proc. Natl. Acad. Sci. USA *92*, 9363–9367.

Giacinti, C., and Giordano, A. (2006). RB and cell cycle progression. Oncogene *25*, 5220–5227.

Halazonetis, T.D., Gorgoulis, V.G., and Bartek, J. (2008). An oncogene-induced DNA damage model for cancer development. Science *319*, 1352–1355.

Hayflick, L., and Moorhead, P.S. (1961). The serial cultivation of human diploid cell strains. Exp. Cell Res. *25*, 585–621.

Katsuno, Y., Suzuki, A., Sugimura, K., Okumura, K., Zineldeen, D.H., Shimada, M., Niida, H., Mizuno, T., Hanaoka, F., and Nakanishi, M. (2009). Cyclin A-Cdk1 regulates the origin firing program in mammalian cells. Proc. Natl. Acad. Sci. USA *106*, 3184–3189.

Kuilman, T., Michaloglou, C., Mooi, W.J., and Peeper, D.S. (2010). The essence of senescence. Genes Dev. *24*, 2463–2479.

Lanni, J.S., and Jacks, T. (1998). Characterization of the p53-dependent postmitotic checkpoint following spindle disruption. Mol. Cell. Biol. *18*, 1055–1064.

Levine, A.J., and Oren, M. (2009). The first 30 years of p53: growing ever more complex. Nat. Rev. Cancer *9*, 749–758.

Lukas, C., Sørensen, C.S., Kramer, E., Santoni-Rugiu, E., Lindeneg, C., Peters, J.M., Bartek, J., and Lukas, J. (1999). Accumulation of cyclin B1 requires E2F and cyclin-A-dependent rearrangement of the anaphase-promoting complex. Nature *401*, 815–818.

Mao, Z., Ke, Z., Gorbunova, V., and Seluanov, A. (2012). Replicatively senescent cells are arrested in G1 and G2 phases. Aging (Albany, N.Y. Online) *4*, 431–435.

Michaloglou, C., Vredeveld, L.C., Soengas, M.S., Denoyelle, C., Kuilman, T., van der Horst, C.M., Majoor, D.M., Shay, J.W., Mooi, W.J., and Peeper, D.S. (2005). BRAFE600-associated senescence-like cell cycle arrest of human naevi. Nature *436*, 720–724.

Nakanishi, M., Robetorye, R.S., Adami, G.R., Pereira-Smith, O.M., and Smith, J.R. (1995). Identification of the active region of the DNA synthesis inhibitory gene p21Sdi1/CIP1/WAF1. EMBO J. *14*, 555–563.

Rayess, H., Wang, M.B., and Srivatsan, E.S. (2012). Cellular senescence and tumor suppressor gene p16. Int. J. Cancer *130*, 1715–1725.

Rowland, B.D., and Bernards, R. (2006). Re-evaluating cell-cycle regulation by E2Fs. Cell *127*, 871–874.

Rufini, A., Tucci, P., Celardo, I., and Melino, G. (2013). Senescence and aging: the critical roles of p53. Oncogene *32*, 5129–5143.

Sage, J., Mulligan, G.J., Attardi, L.D., Miller, A., Chen, S., Williams, B., Theodorou, E., and Jacks, T. (2000). Targeted disruption of the three Rb-related genes leads to loss of G(1) control and immortalization. Genes Dev. *14*, 3037–3050.

Sakaue-Sawano, A., Kurokawa, H., Morimura, T., Hanyu, A., Hama, H., Osawa, H., Kashiwagi, S., Fukami, K., Miyata, T., Miyoshi, H., et al. (2008). Visualizing spatiotemporal dynamics of multicellular cell-cycle progression. Cell *132*, 487–498.

Shay, J.W., Pereira-Smith, O.M., and Wright, W.E. (1991). A role for both RB and p53 in the regulation of human cellular senescence. Exp. Cell Res. *196*, 33–39.

Spencer, S.L., Cappell, S.D., Tsai, F.C., Overton, K.W., Wang, C.L., and Meyer, T. (2013). The proliferation-quiescence decision is controlled by a bifurcation in CDK2 activity at mitotic exit. Cell *155*, 369–383.

Takahashi, A., Imai, Y., Yamakoshi, K., Kuninaka, S., Ohtani, N., Yoshimoto, S., Hori, S., Tachibana, M., Anderton, E., Takeuchi, T., et al. (2012). DNA damage signaling triggers degradation of histone methyltransferases through APC/C(Cdh1) in senescent cells. Mol. Cell *45*, 123–131.

Uetake, Y., and Sluder, G. (2004). Cell cycle progression after cleavage failure: mammalian somatic cells do not possess a "tetraploidy checkpoint". J. Cell Biol. *165*, 609–615.

Vodermaier, H.C. (2004). APC/C and SCF: controlling each other and the cell cycle. Curr. Biol. *14*, R787–R796.

Wiebusch, L., and Hagemeier, C. (2010). p53- and p21-dependent premature APC/C-Cdh1 activation in G2 is part of the long-term response to genotoxic stress. Oncogene *29*, 3477–3489.

Wong, C., and Stearns, T. (2005). Mammalian cells lack checkpoints for tetraploidy, aberrant centrosome number, and cytokinesis failure. BMC Cell Biol. *6*, 6.

Ye, C., Zhang, X., Wan, J., Chang, L., Hu, W., Bing, Z., Zhang, S., Li, J., He, J., Wang, J., and Zhou, G. (2013). Radiation-induced cellular senescence results from a slippage of long-term G2 arrested cells into G1 phase. Cell Cycle *12*, 1424–1432.

Cancer Research

CBP-93872 Inhibits NBS1-Mediated ATR Activation, Abrogating Maintenance of the DNA Double-Strand Break–Specific G_2 Checkpoint

Takahisa Hirokawa[1,2], Bunsyo Shiotani[3], Midori Shimada[1], Kazuhiro Murata[1], Yoshikazu Johmura[1], Mayumi Haruta[1], Hidetoshi Tahara[3], Hiromitsu Takeyama[2], and Makoto Nakanishi[1]

Abstract

CBP-93872 was previously identified as a G_2 checkpoint inhibitor using a cell-based high-throughput screening system. However, its molecular actions as well as cellular targets are largely unknown. Here, we uncovered the molecular mechanisms underlying abrogation of the G_2 checkpoint by CBP-93872. CBP-93872 specifically abrogates the DNA double-stranded break (DSB)–induced G_2 checkpoint through inhibiting maintenance but not initiation of G_2 arrest because of specific inhibition of DSB-dependent ATR activation. Hence, ATR-dependent phosphorylation of Nbs1 and replication protein A 2 upon DSB was strongly suppressed in the presence of CBP-93872. CBP-93872 did not seem to inhibit DNA-end resection, but did inhibit Nbs1-dependent and ssDNA-induced ATR activation *in vitro* in a dose-dependent manner. Taken together, our results suggest that CBP-93872 is an inhibitor of maintenance of the DSB-specific G_2 checkpoint and thus might be a strong candidate as the basis for a drug that specifically sensitizes p53-mutated cancer cells to DSB-inducing DNA damage therapy. *Cancer Res; 74(14); 3880–9. ©2014 AACR.*

Introduction

Maintaining the genomic stability of both normal cells and cancer cells depends on coordinated networks of different forms of the DNA damage response, which execute various cell activities such as cell-cycle arrest, apoptosis, and premature senescence (1). Abrogation of these systems likely leads to extensive genomic instability and subsequent cell death upon DNA damage. Cell-cycle arrest in response to DNA damage plays a key role in increasing cell survival and is mediated in mammals by at least two distinct pathways; one via ATM-p53-p21 (2, 3) and the other via ATM/ATR-Chk1-Cdc25 (4, 5). The former mediates both G_1 and G_2 arrest and the latter mediates G_2 arrest (6–8). Given that most cancer cells have genetic alterations in p53, their survival in the presence of DNA damage depends on a functional Chk1-mediated G_2 checkpoint, suggesting that reagents capable of inhibiting this checkpoint would be promising drugs for producing synthetic lethality to p53-deficient cancer cells.

Authors' Affiliations: Departments of [1]Cell Biology and [2]Gastroenterological Surgery, Graduate School of Medical Sciences, Nagoya City University, Mizuho-cho, Mizuho-ku, Nagoya; and [3]Department of Cellular and Molecular Biology, Hiroshima University, Hiroshima, Japan

Note: Supplementary data for this article are available at Cancer Research Online (http://cancerres.aacrjournals.org/).

Corresponding Author: Makoto Nakanishi, Department of Cell Biology, Graduate School of Medical Sciences, Nagoya City University, 1 Kawasumi, Mizuho-cho, Mizuho-ku, Nagoya 467-8601, Japan. Phone: 81-52-853-8144; Fax: 81-52-842-3955; E-mail: mkt-naka@med.nagoya-cu.ac.jp

doi: 10.1158/0008-5472.CAN-13-3604

Signals initiated by DNA damage sensors are rapidly transduced to downstream targets in a manner dependent on the type of damage. For example, signals from DNA double-stranded break (DSB) sensors are rapidly transduced to an ataxia telangiectasia mutated (ATM) kinase (9) and a DNA-dependent protein kinase catalytic subunit (DNA-PKcs) that in turn leads to the processing of DSBs by nucleases generating an ATR-activating structure (10–12). In contrast, a broad spectrum of DNA damage changes, such as a structure consisting of single-stranded DNA (ssDNA) and a junction between ssDNA and double-stranded DNA (dsDNA), can directly activate ATM- and Rad3-related (ATR) kinases in a replication protein A (RPA)- and Rad17-dependent manner, respectively (13). The activated ATM and/or ATR transduce the damage signals to a large number of downstream effectors, such as p53, Chk1, and Chk2, and execute G_1 and G_2 DNA damage checkpoints (1).

On the basis of the absolute requirement for the G_2 DNA damage checkpoint for p53-deficient cancer cell survival upon DNA damage, various G_2 checkpoint inhibitors have been developed and proposed for clinical application. Among them, caffeine is one of the most extensively investigated agents that inhibits ATM and ATR kinases and increases sensitization of p53-deficient cells to IR irradiation. Chk1 inhibitors, such as UCN-01 (14), CEP-3891 (15), and AZD7762 (16) are also proposed to be potent G_2 checkpoint suppressors. However, the kinases ATR and Chk1 are essential for mammalian cell survival (17–21) and ATM is also required for maintaining genomic integrity during normal cell growth (22). Therefore, these drugs would have unexpected deleterious effects on normal cell function, diminishing the possibility of their clinical application.

We have previously identified CBP-93872 as a promising G_2 checkpoint inhibitor using a high-throughput screening system that detected abrogation of the G_2 checkpoint in IR-irradiated HT-29 cells (23). However, molecular mechanisms underlying G_2 checkpoint inhibition by this drug are largely unknown. Importantly, treatment with this drug markedly sensitized p53-mutated cancer cells to DSB-inducing DNA damaging agents. In this study, we investigated the molecular basis of G_2 checkpoint inhibition by CBP-93872 in p53-deficient cancer cells and found that CBP-93872 specifically inhibited DSB-mediated and Nbs1-dependent activation of ATR.

Materials and Methods

Cell culture and drug treatment

HT29 and HCT116 cells were grown in McCoy's 5A (Gibco) supplemented with 10% fetal bovin serum (FBS) and 1% penicillin–streptomycin (Invitrogen). NCI-H460, A549 and MCF7 cells were cultured in RPMI-1640 (Sigma-Aldrich) supplemented with 10% FBS and 1% penicillin–streptomycin. All cells were cultured at 37 °C under 5% CO_2.

Inhibitors used in this study were as follows: CBP-93872 (20 μmol/L; kindly supplied by Chugai Pharmaceutical Co., Ltd.), UCN01 (300 nmol/L; Sigma-Aldrich), caffeine (2 mmol/L; Sigma-Aldrich), KU-55933 (20 μmol/L; Sigma-Aldrich), and Nocodazole (500 nmol/L; Sigma-Aldrich).

MMS (Sigma-Aldrich) was used at 200 μmol/L and hydroxyurea (Sigma-Aldrich) was used at different concentrations.

Plasmid construction

To generate lentivirus shRNA constructs, an shRNA-coding fragment with a 5′-ACGTGTGCTGTCCGT-3′ loop was digested into pENTER4-H1tetOx1 (a gift of H. Miyoshi). To insert the H1tetOx1-shRNA into a lentivirus vector, the vector pENTER4-H1tetOx1-shRNA was mixed with CS-RFA-ETBsd (a gift of H. Miyoshi) and treated with Gateway LR clonase (Invitrogen).

The full-length cDNA of wild-type human Nbs1 was obtained by RT-PCR, and ligated into pcDNA3.1-myc-His vector. To construct Tet-on inducible lentivirus vectors, a cDNA fragment of Nbs1 containing the myc-His epitope was inserted into a pENTER1A vector (Invitrogen). shRNA-resistant mutations and an EDE mutation of pENTR1A Nbs1-myc-His were generated by inverse PCR with a Site-Specific Mutagenesis Kit (Toyobo). The resultant plasmids were mixed with CS-IV-TRE-RfA-UbC-Puro vector (a gift of H. Miyoshi), and treated with Gateway LR clonase to generate the lentivirus vectors.

Virus generation and infection

Lentiviruses expressing the respective shRNAs were generated by cotransfection of 293T cells with pCMV-VSV-G-RSV-RevB (a gift of H. Miyoshi), pCAG-HIVgp (a gift of H. Miyoshi), and the respective CS-RFA-ETBsd using the calcium phosphate coprecipitation method. HT29 cells infected with the viruses were treated with 10 μg/mL blasticidin (Invitrogen) for 3 days.

For the generation of cells depleted of endogenous Nbs1 and expressing ectopic Nbs1Wt-myc-His or Nbs1EDE-myc-His, HT29 cells expressing shNbs1 were infected with lentiviruses expressing pENTR1A Nbs1Wt-myc-His or pENTR1A Nbs1EDE-myc-His containing an shRNA-resistant mutation. Infected cells were treated with 10 μg/mL blasticidin and 2 μg/mL of puromycin (Sigma-Aldrich).

To express the inducible shRNA and gene, doxycycline (Sigma-Aldrich) was incubated in the medium at a concentration of 1 μg/mL for 3 days.

shRNA target sequences

The targeting sequences used in preparing shRNA were as follows: ATR, GCCGCTAATCTTCTAACATTA; CtIP, GCATCATCCTTCAGCCCTTGA; Nbs1, GGAGGAAGATGTCAATGTTAG; and control, CGTACGCGGAATACTTCGA.

Measurement of mitotic indices

Cells were treated with IR, UV, or MMS, and fixed with 70% ethanol at specific times. Nocodazole was added 1 hour after treatment. Fixed cells were then stained with antibodies to phospho-histone H3 at S10 (H3 pS10; 1:200; Millipore) for 1 hour, followed by 30-minute incubation with Alexa Fluor 488 secondary antibodies (1:100; Invitrogen). DNA was counterstained with 0.1 mg/mL propidium iodide containing RNase for 30 minutes at 37 °C. Flow cytometry was performed using a FACSCanto II flow cytometer (BD Biosciences).

Antibodies

Antibodies used in this study are listed in Supplementary Table S1.

Immunoblotting

For preparation of whole cell extracts, cells were lysed with immunoprecipitation kinase buffer (50 mmol/L HEPES, pH 8.0, 150 mmol/L NaCl, 2.5 mmol/L EGTA, 1 mmol/L EDTA 1 mmol/L DTT, 0.1% Tween 20, 10% glycerol) containing a cocktail of protease and phosphatase inhibitors. Cell lysates were boiled with SDS sample buffer (45 mmol/L Tris-HCl, pH 6.8, 10% glycerol, 1% SDS, 0.01% bromophenol blue, 50 mmol/L DTT). Proteins in the lysates were separated by SDS-PAGE and transferred onto polyvinylidene difluoride membranes. Membranes were incubated overnight with primary antibodies, followed by 1 hour incubation with horseradish peroxidase–conjugated secondary antibodies.

Immunoprecipitation

Immunoprecipitation was performed essentially as previously described (24). For immunoprecipitation, cells were lysed in immunoprecipitated kinase buffer containing a cocktail of protease and phosphatase inhibitors. Cell lysates were incubated with primary antibodies at 4 °C for overnight, followed by incubation with protein G-agarose (GE Healthcare) for 1 hour. Immunoprecipitates were thoroughly washed three times with immunoprecipitation kinase buffer and resuspended in 2× SDS sample buffer.

Immunohistochemical analysis

Cells on cover slips were fixed in 4% paraformaldehyde for 10 minutes at room temperature, permeabilized with 0.5% Triton X-100 in PBS for 10 minutes, and incubated in blocking buffer

(PBS + 5% bovine serum albumin + 0.1% Tween 20) for 30 minutes. The cells on the slips were then incubated with anti-RPA2 and anti-γ-H2AX antibodies diluted in blocking buffer (1:500) for 2 hours at room temperature, followed by incubation with anti-rat IgG conjugated with Alexa Fluor 488 (Life Technologies) and anti-rabbit IgG conjugated with Alexa Fluor 594 (Life Technologies) secondary antibodies diluted in blocking buffer (1:400) for 1 hour at room temperature. Nuclei were counterstained with Hoechst 33342 (1:1,000).

In vitro kinase assay

ATR kinase assays were performed essentially as previously described (25) with the following modifications. HEK293E cells were transfected with Flag-ATR– and His-ATRIP–expressing plasmids, and Flag-ATR was immunoprecipitated with anti-Flag M2 antibody in TGN buffer [50 mmol/L Tris-HCl (pH 7.5), 150 mmol/L NaCl, 50 mmol/L phosphoglycerol, 10% glycerol, 1% Tween 20, 1 mmol/L phenylmethylsulfonyl fluoride (PMSF), 1 mmol/L NaF, 1 mmol/L Na_3VO_4, 1 mmol/L DTT, and protease inhibitors]. The precipitates were washed twice with the TGN buffer, once with the TGN buffer supplemented with 0.5 M LiCl, and twice with the reaction buffer [10 mmol/L HEPES (pH 7.5), 50 mmol/L NaCl, 10 mmol/L $MgCl_2$, 50 mmol/L glycerophosphate, 1 mmol/L DTT, and protease inhibitors] without ATP. The *in vitro* kinase reactions were conducted in the presence of 50 μmol/L ATP and purified GST-Rad17. Phosphorylation of Rad17 was monitored using phospho-Rad17 (Ser645) antibody (Bethyl).

Preparation of nuclear extracts

HCT116 cells were grown to ≤80% confluence, trypsinized, and centrifuged (200 × *g* for 3 minutes at room temperature), then washed in PBS. The cell pellets were suspended in a 5× packed cell volume of hypotonic buffer A (10 mmol/L Hepes-KOH, pH 7.9, 10 mmol/L KCl, 1.5 mmol/L $MgCl_2$, 0.5 mmol/L DTT, and 0.5 mmol/L PMSF) supplemented with a cocktail of protease inhibitors (Nakalai Tesque) and incubated on ice for 5 minutes. Cells were then centrifuged at 500 × *g* for 5 minutes at 4°C, suspended in a 2× packed cell volume of buffer A and lysed by Dounce homogenization using a tight-fitting pestle. Nuclei were collected as a pellet by centrifugation at 4,000 × *g* for 5 minutes at 4°C and extracted in an equal volume of buffer C (20 mmol/L Hepes-KOH, pH 7.9, 600 mmol/L KCl, 1.5 mmol/L $MgCl_2$, 0.2 mmol/L EDTA, 25% glycerol, 0.5 mmol/L DTT, and 0.5 mmol/L PMSF) supplemented with a protease cocktail, and mixed on a rotator at 4°C for 30 minutes. Nuclear extracts (supernatants) were recovered by centrifugation (16,000 × *g* for 15 minutes at 4°C) and dialyzed using Slide-A-Lyzer Dialysis Cassettes (3,500-D protein molecular weight cutoff; Thermo Fisher Scientific) against buffer D (20 mmol/L Hepes-KOH, pH 7.9, 100 mmol/L KCl, 0.2 mmol/L EDTA, 20% glycerol, 0.5 mmol/L DTT, and 0.5 mmol/L PMSF). Dialyzed nuclear extracts were centrifuged (16,000 × *g* for 30 minutes at 4°C) to eliminate residual precipitates. The protein concentration of the clear supernatant was determined using Bradford's estimation method, and aliquots were snap frozen and stored at −80°C.

Extract-based ATR activation assay

An extract-based ATR activation assay was performed essentially as previously described (26) with the following modifications. Nuclear extracts were pretreated with 10 mmol/L of KU-55933 and NU7026 (Sigma-Aldrich) for 15 minutes on ice to inhibit ATM and DNA-PKcs, and supplemented with the reaction buffer (buffer R), which brought the final buffer compositions to 10 mmol/L HEPES (pH 7.6), 50 mmol/L KCl, 0.1 mmol/L $MgCl_2$, 1 mmol/L phenylmethanesulfonylfluoride, 0.5 mmol/L dithiothreitol, 1 mmol/L ATP, 10 mg/mL creatine kinase, and 5 mmol/L phosphocreatine. ssDNA (70nt) or ssDNA/dsDNA junction were incubated with the extracts for 15 minutes at 37 °C.

Sequences of DNA oligonucleotides

ss50: 5′-AGCGCCCAATACGCAAACCGCCTCTCCCCGCGCGTTGGCCGA
TTCATTAA-3′

ss70: 5′-TGCAGCTGGCACGACAGGTTTTAATGAATCGGCCAACGCGCG
GGGAGAGGCGGTTTGCGTATTGGGCGCT-3′.

Results

CBP-93872 specifically suppresses the DSB-induced G_2 checkpoint

To clarify the molecular basis of G_2 checkpoint abrogation by CBP-93872 (Fig. 1A), we first examined whether the effect of this drug on the G_2 checkpoint was dependent on the type of DNA damage. HT-29 cells lacking functional p53 were treated with IR, UV, or MMS in the presence or absence of CBP-93872, and the cell cycle before entry into mitosis arrest was evaluated by determining mitotic indices using phospho-histone H3 at serine 10 (H3 pS10) as a mitotic marker. CBP-93872 effectively suppressed G_2 arrest induced by IR treatment whereas it did not affect that induced by UV or MMS (Fig. 1B). In contrast, UCN-01 effectively suppressed G_2 arrest induced by UV and MMS. Consistent with this, upon IR treatment, Chk1 phosphorylation at serines 317 and 345 was notably compromised in the presence of CBP-93872 (Fig. 1C). Interestingly, CBP-93872 did not suppress ATM activation (phosphorylation of ATM at S1981; ATM pS1981) and subsequent phosphorylation of Chk2 after IR treatment. In addition, this drug did not affect Chk1 phosphorylation upon UV, MMS, or HU treatment (Fig. 1D–F). Taken together, these results suggested that the cellular target of CBP-93872 should exist downstream of DSB-induced ATM activation.

CBP-93872 does not inhibit initiation but does inhibit maintenance of the DSB-induced G_2 checkpoint

To examine the mode of G_2 checkpoint suppression by CBP-93872, we examined the percentage of H3 pS10-positive cells by flow cytometry. Mitotic indices, in the presence of CBP-93872, of HT29, A549, and NCI-H460 cells were significantly decreased at 1 hour after IR treatment, but increased at 16 hours (Fig. 2A). In contrast, reduction of these indices in the presence of caffeine or UCN-01 was only minimal at 1 hour and markedly increased at 12 hours. In MCF7 cells that possess functional

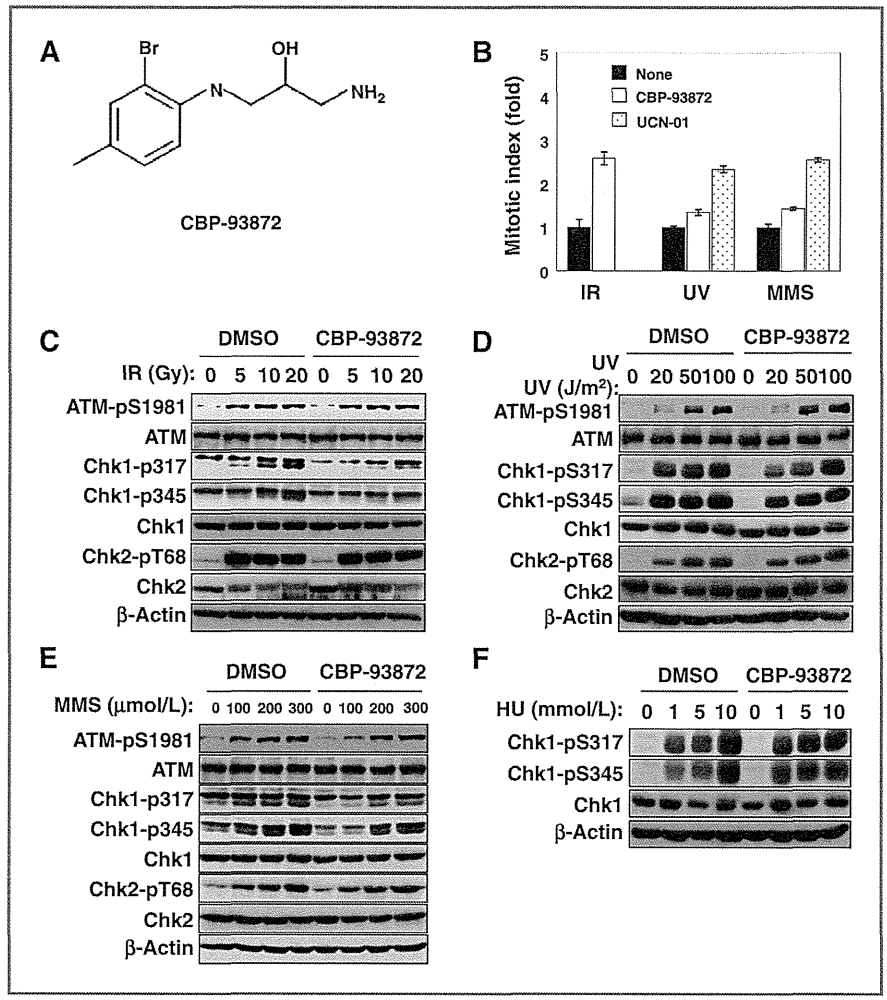

Figure 1. CBP-93872 specifically abrogated the IR-induced G_2 checkpoint. A, chemical structure of CBP-93872. B, HT29 cells were treated with IR (10 Gy), UV (10 J/m^2), or MMS (200 μmol/L). Eight hours after treatment, cells were then incubated in the presence or absence of CBP-93872 (20 μmol/L) or UCN01 (300 nmol/L). Nocodazole (500 nmol/L) was simultaneously added to prevent cells from exiting mitosis. Cells were fixed 8 hours after treatment and subjected to FACS analysis. Mitotic cells were determined to be positive for phospho-histone H3 at S10 (pS10) and relative mitotic indices are expressed as a multiple of those without inhibitors. Data are presented as means ± SD of at least three independent experiments. HT29 cells were treated with the indicated doses of IR (C), UV (D), MMS (E), or hydroxyurea (HU; F) in the presence or absence of CBP-93872 (20 μmol/L). Two hours (IR, UV, and MMS) or 4 hours (HU) after treatment, cells were harvested and whole cell extracts were subjected to immunoblotting using the indicated antibodies.

p53, mitotic indices in the presence of CBP-93872 were continuously low. These results suggested that CBP-93872 abrogates maintenance of the G_2 checkpoint, but not its initiation, whereas caffeine and UCN-01 inhibit both its initiation as well as its maintenance. Consistent with this, immunoblotting revealed that the level of H3 pS10 in the presence of CBP-93872 was reduced at 4 hours and was elevated again at 8 hours after IR treatment (Fig. 2B). In contrast, the levels of H3 pS10 were almost constant in the presence of UCN-01 and KU-55933, an ATM-specific inhibitor. As expected, KU-55933 inhibited IR-induced ATM pS1981 and subsequent phosphorylation of Chk2. UCN-01 did not inhibit IR-induced ATM pS1981 and Chk2 phosphorylation, but rather enhanced Chk1 phosphorylation at S317 and S345.

CBP-93872 suppresses DSB-induced ATR activation

We then examined whether CBP-93872 was inhibitory upstream or downstream of ATR activation. ATR activation was detected by its auto-phosphorylation at T1989 (25). Immunoblotting analysis revealed that phospho-ATR at T1989 as well as Chk1 phosphorylation were readily detected after doses of 1 Gy or more IR treatment (Fig. 3A). CBP-93872 strongly inhibited DSB-induced ATR activation and subsequent Chk1 phosphorylation. Importantly, UV treatment activated ATR in a dose-dependent manner and this activation as well as UV-induced Chk1 phosphorylation were not affected by the treatment with CBP-93872 (Fig. 3B). Treatment with CBP-93872 did not affect S-phase progression with or without UV treatment, eliminating the possibility that the inability of CBP-93872 to inhibit UV-induced Chk1 phosphorylation was an indirect consequence of an altered progression of S phase (Supplementary Fig. S1). We then examined whether CBP-93872 directly inhibited ATR activity. An *in vitro* kinase assay using recombinant wild-type ATR and ATRIP complex revealed that CBP-93872, even at a maximum concentration (200 μmol/L), failed to inhibit ATR activity whereas VE-821, an ATR-specific inhibitor, did so effectively, indicating that CBP-93872 is not a direct inhibitor of ATR (Fig. 3C). Taken together, a molecular target of CBP-93872 should exist during the process occurring between ATM-dependent

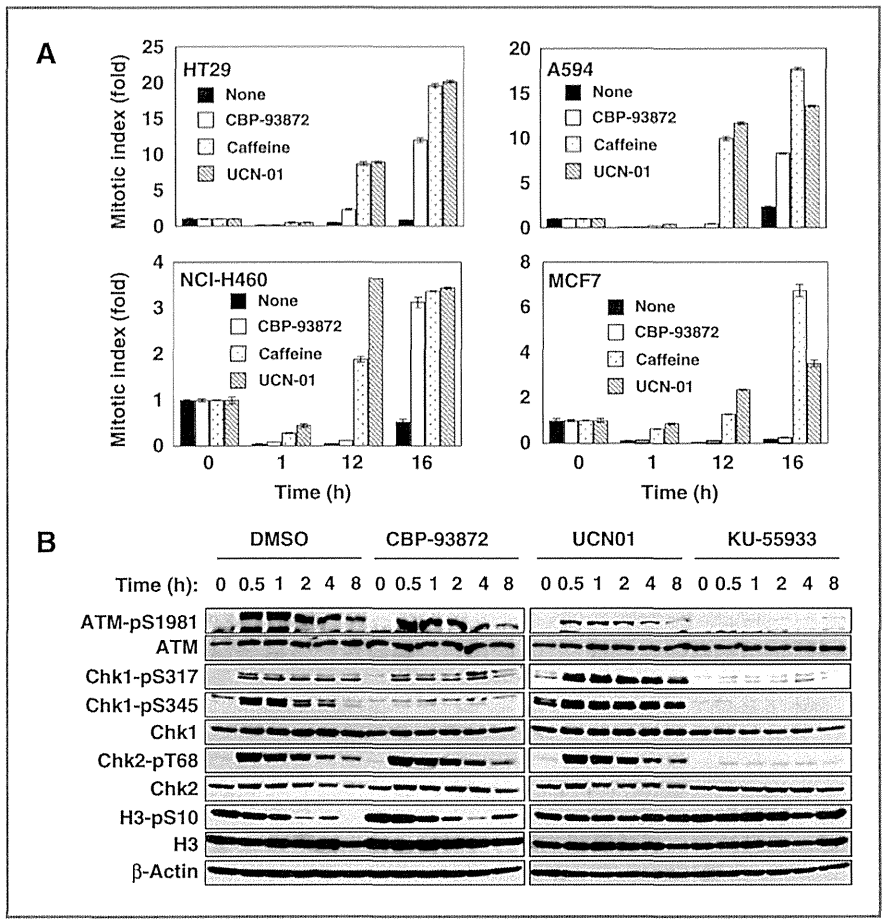

Figure 2. CBP-93872 abrogated maintenance, but not initiation, of the DSB-induced G_2 checkpoint. A, p53-deficient HT29, A549, and NCI-H460 cells and p53-positive MCF7 cells were treated with IR (10 Gy) in the presence of either DMSO (control), CBP-93872 (20 μmol/L), caffeine (2 mmol/L), or UCN01 (300 nmol/L). One hour after IR treatment, nocodazole (500 nmol/L) was added to cells as in Fig. 1B and cells were fixed at the indicated times. Fixed cells were then subjected to FACS analysis. Mitotic indices were determined as in Fig. 1B and data are presented as means ± SD of at least three independent experiments. B, HT29 cells were treated with IR (10 Gy) in the presence of DMSO (control), CBP-93872 (20 μmol/L), UCN01 (300 nmol/L), or KU-55933 (20 μmol/L). Cells were harvested at the indicated times after irradiation and whole cell extracts were subjected to immunoblotting using the indicated antibodies.

generation of the ATR-activating DNA structure and ATR activation.

CBP-93872 did not inhibit DNA-end resection at DSB sites

ATR activation in response to DSB requires conversion of ATM-activating DSB structures into ATR-activating structures (25, 26). DNA-ends at DSBs sites are rapidly processed by nucleases in combination with CtIP, generating ssDNA and a junction between ssDNA and dsDNA (27). ssDNA is bound by RPA, forming nuclear foci. Therefore, we used an immunohistochemical analysis using anti-RPA2 antibodies to determine whether CBP-93872 blocked DNA-end resection at DSB sites. In control cells, RPA2 foci formation was readily detectable after IR treatment. These nuclear foci were colocalized with γH2AX foci, suggesting that RPA2 foci represented ssDNA regions generated by DNA-end resection at DSB sites. Depletion of CtIP almost completely compromised RPA2 foci formation (Fig. 4A). In contrast, RPA2 foci were readily detectable in cells treated with CBP-93872. Interestingly, in response to DSB, depletion of CtIP showed an abrogation of the G_2 checkpoint similar to that upon treatment with CBP-93872 (28). Depletion of CtIP did not inhibit ATM autophosphorylation at S1981, but it did compromise Chk1 phosphorylation at S317 and S345 and RPA2 phosphorylation (Fig. 4B). As with the CBP-93872 treatment, DNA-end resection at DSB sites seemed to be required for maintenance of the G_2 checkpoint in response to DSB (Fig. 4C). These results suggested that molecular targets of CBP-93872 exist between DNA-end resection and ATR activation.

CBP-93872 inhibited ATR-dependent phosphorylation of Nbs1 at S343

Importantly, checkpoint activation, which is evaluated by Chk1 phosphorylation, seemed to be dependent on either Nbs1 or Rad17 depending on the type of DNA damage. On UV treatment, Chk1 phosphorylation at S317 and S345 was almost completely abrogated when Rad17, but not Nbs1, was depleted, whereas on IR treatment these phosphorylations were dependent on the presence of Nbs1 but not Rad17 (Supplementary Fig. S2). Treatment with CBP-93872 specifically inhibited NBS1-dependent, but not Rad17-dependent phosphorylation of Chk1 at S317 and S345 upon IR treatment, showing that the inhibitory effect of CBP-93872 was only a minimal in cells depleted of Nbs1. Consistent with this, 2 distinct modes of ATR activation have been recently proposed (29, 30). One is dependent on Rad17-TopBP1 circuitry and the other is dependent on the ssDNA-bound MRN complex. The former has been

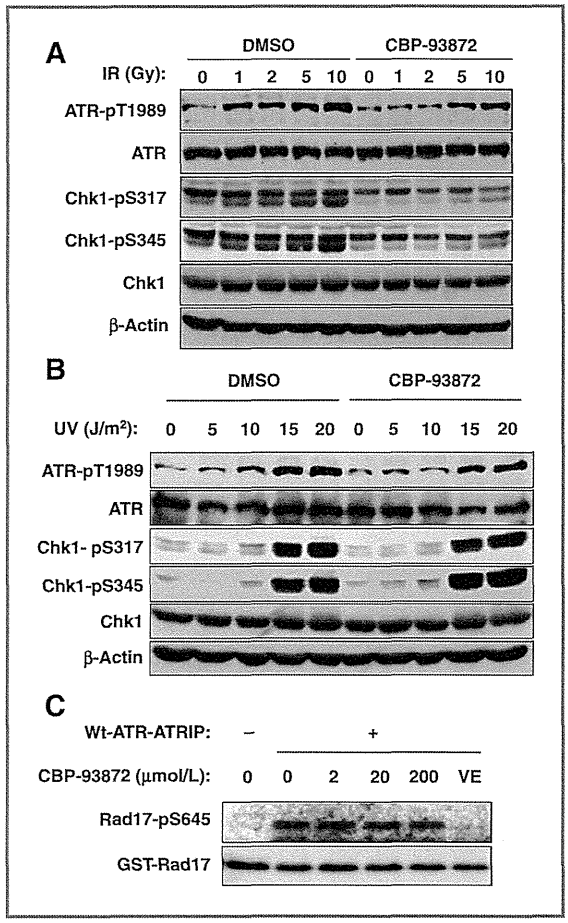

Figure 3. CBP-93872 specifically inhibited DSB-induced ATR activation. HT29 cells were treated with the indicated doses of IR (A) or UV (B) in the presence of DMSO or CBP-93872 (20 μmol/L). Cells were harvested at 2 hours after irradiation and WCEs were subjected to immunoblotting using the indicated antibodies. C, *in vitro* kinase assay using recombinant ATR-ATRIP complex and purified GST-Rad17 protein as a substrate. GST-Rad17 was incubated with or without purified wild-type-ATR-ATRIP (Wt-ATR-ATRIP) complex at 37°C for 30 minutes in the presence of the indicated concentration of CBP-93872 (20 μmol/L) or VE-821 (10 μmol/L). Kinase activity was stopped by boiling with SDS sample buffer, and phosphorylation of Rad17 at Ser645 was analyzed by immunoblotting using the specific antibodies (pRad17 Ser645).

proposed to be involved in mechanisms underlying initiation of ATR checkpoint signaling on a junction between ssDNA and double-stranded DNA, and the latter to be involved in the mechanism by which the ATR checkpoint signal is amplified on ssDNA. Therefore, we hypothesized that DSB-induced phosphorylation of Nbs1 at S343 was at least in part caused by activated ATR during amplification of the checkpoint signal. As shown in Fig. 5A, depletion of ATR strongly suppressed IR-induced Nbs1 phosphorylation at S343. Intriguingly, treatment with CBP-93872 also markedly inhibited this phosphorylation. Analysis of the kinetics of DSB-induced Nbs1 phosphorylation revealed that phosphorylation increased at 2 hours and reached a maximum at 4 to 8 hours, which was inhibited by CBP-93872 (Fig. 5B), suggesting that this phosphorylation is involved in the maintenance but not the initiation of the G_2 checkpoint. Importantly, CBP-93872 did not affect the complex formation of Nbs1 with Mre11 and Rad50 (Fig. 5B and C). CBP-93872 specifically inhibited IR-induced, but not UV-induced Nbs1 phosphorylation (Fig. 5C).

An Nbs1 mutant lacking RPA binding showed a defect in maintenance of the G_2 checkpoint

Given that RPA binding of Nbs1 is required for MRN-mediated ATR activation (29), we asked whether an Nbs1 mutant lacking RPA binding (EDE mutant) would exhibit a defect in the maintenance of the G_2 checkpoint as with CBP-93872 treatment. Depletion of Nbs1 resulted in the defect in initiation and maintenance of the G_2 checkpoint, as shown by the fact that the mitotic index was not decreased at 1 hour and was increased at 24 hours after IR treatment (Fig. 5D). Ectopic expression of wild-type Nbs1 in endogenous Nbs1-depleted cells restored the ability to arrest the cell cycle before mitosis, even at 24 hours after treatment. In contrast, as with CBP-93872 treatment, expression of the EDE mutant restored the ability to initiate G_2 arrest in response to DSB, but failed to maintain it. Consistent with this, as with CBP-93872 treatment, expression of the EDE mutant restored autophosphorylation of ATM (ATM pS1981) at 1 hour, but failed in phosphorylation of Chk1 at S345 at 24 hours (Fig. 5E). Complex formation of the EDE mutant with Mre11 and Rad50 was confirmed by immunoprecipitation-immunoblotting analysis using Mre11 immunoprecipitates (Fig. 5F). Taken together, these results indicated that a defect in MRN-dependent activation of ATR had a similar phenotype to that seen with CBP-93872 treatment.

CBP-93872 directly inhibited ssDNA-induced ATR activation *in vitro*

Finally, we examined whether CBP-93872 suppressed amplification of ATR checkpoint signaling on ssDNA or the ssDNA/dsDNA junction using a recently developed *in vitro* assay (29). In this system, ssDNA or the ssDNA/dsDNA junction alone when incubated with nuclear extract was sufficient to induce RPA2 S33 phosphorylation and this phosphorylation was dependent upon ATR, TopBP1, and Nbs1. CBP-93872 inhibited RPA2 phosphorylation at S33 in the nuclear extract incubated with ssDNA in a dose-dependent manner (Fig. 6A, left). However, CBP-93872 did not affect RPA phosphorylation at S33 in the extract incubated with the ssDNA/dsDNA junction (Fig. 6A, right). In addition, treatment with CBP-93872 in HT29 cells strongly suppressed RPA2 phosphorylation at S33 (Fig. 6B). Taken together, these results suggested that CBP-93872 directly inhibited amplification of ATR checkpoint signaling by suppressing ssDNA-dependent activation of ATR.

Discussion

Numerous G_2 checkpoint inhibitors have been developed and many have been proposed as potent candidates for DSB sensitization of p53-deficient cancer cells on the basis of the concept that survival of p53-mutated cancer cells relies on the

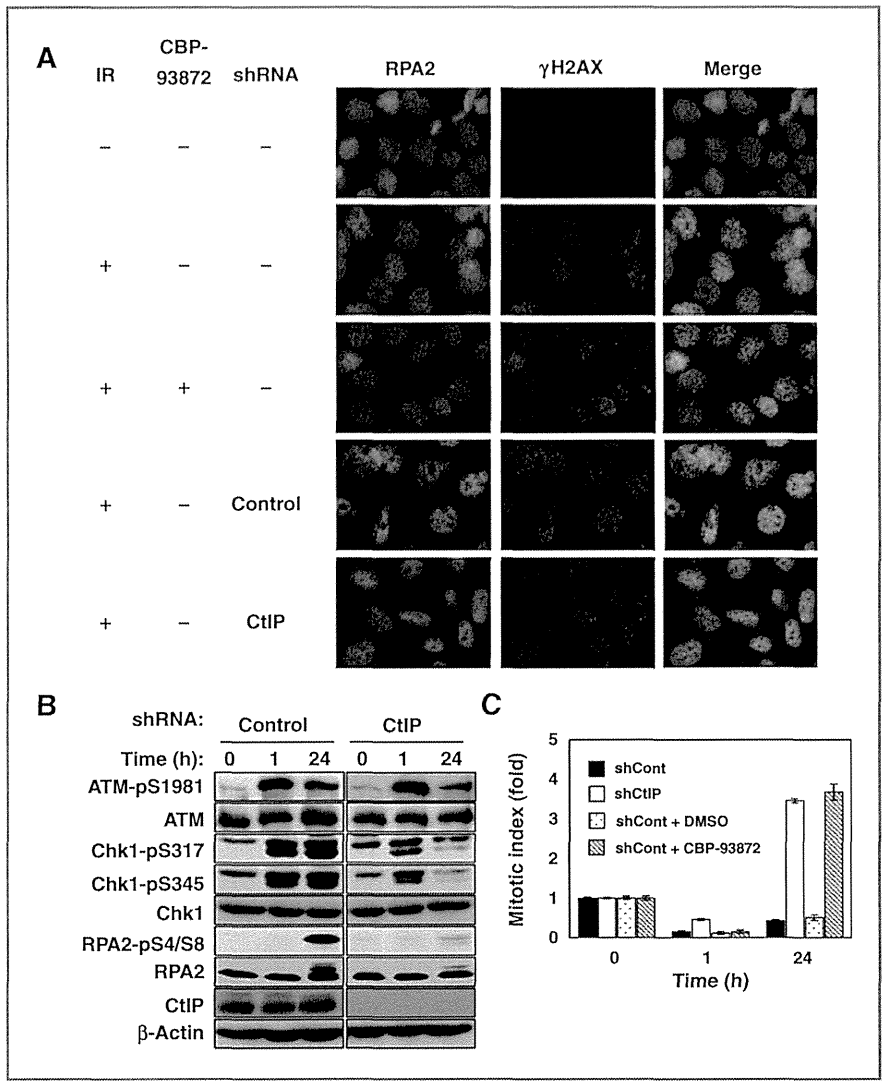

Figure 4. CBP-93872 did not affect IR-induced formation of RPA2 nuclear foci. A, HT29 cells were infected with Tet-on inducible lentiviruses expressing shControl or shCtIP. Infected cells were cultured in the presence of doxycycline (1 μg/mL) for 3 days. Cells were then treated with or without IR (10 Gy) in the presence or absence of CBP-93872 (20 μmol/L). Four hours after irradiation, cells were fixed and stained with anti-RPA2 and anti-γH2AX antibodies. Images were captured by fluorescence microscopy. Cells expressing shControl and shCtIP cells were irradiated with IR (10 Gy) as in A. Nocodazole (500 nmol/L) was added at 1 hour after IR and cells were collected at the indicated times. Whole cell extracts were subjected to immunoblotting using the indicated antibodies (B). Fixed cells were stained with anti-histone H3 pS10 antibodies and mitotic indices were determined as in Fig. 2A. Data are presented as means ± SD of at least three independent experiments (C).

Chk1-mediated G_2 checkpoint upon DSB. For example, Chk1 seems to be a promising target because this kinase is essential for G_2 arrest in response to various genotoxic stressors. Several small molecules exhibiting inhibitory activity toward Chk1 have been identified, such as UCN-01 (14). ATM and ATR are also candidates as targets of G_2 checkpoint inhibitors. In addition, a Wee1 inhibitor, MK-1775, has been developed as a potentiator of DNA damage caused by cytotoxic chemotherapy (31). However, the majority of these inhibitors interact with the ATP binding site of the kinase and it would be difficult to obtain highly selective ATP-competitive kinase inhibitors as the ATP binding site has a very similar structure in all kinases. Furthermore, in normal cells, most of their molecular targets play a key role in the survival and maintenance of genomic integrity. Therefore, these inhibitors can easily cause unexpected deleterious effects on normal cell function, diminishing the possibility of their clinical application.

To obtain G_2 checkpoint inhibitors with a novel mode of action, a high-throughput screening system using p53-deficient HT29 cells was used and CBP-93872 was identified as a potential candidate for use as a G_2 checkpoint inhibitor, although the molecular mechanisms underlying this inhibition are largely unknown. In this study, we found that CBP-93872 inhibited ATR activation specifically following DSB. ATR activation in response to DSB requires ATM activation and the subsequent processing of DSB ends by nucleases, generating ssDNA regions and ssDNA/dsDNA junctions that function as ATR-activating structures. Importantly, although ATR and ATM themselves play key roles in cell survival and maintenance of genomic integrity, respectively, during the normal cell cycle (19, 22), the molecular pathway between ATM activation and ATR activation seems not to be essential for normal cell growth. Therefore, molecules that target this pathway would be most the desirable for use as drugs, because they have far

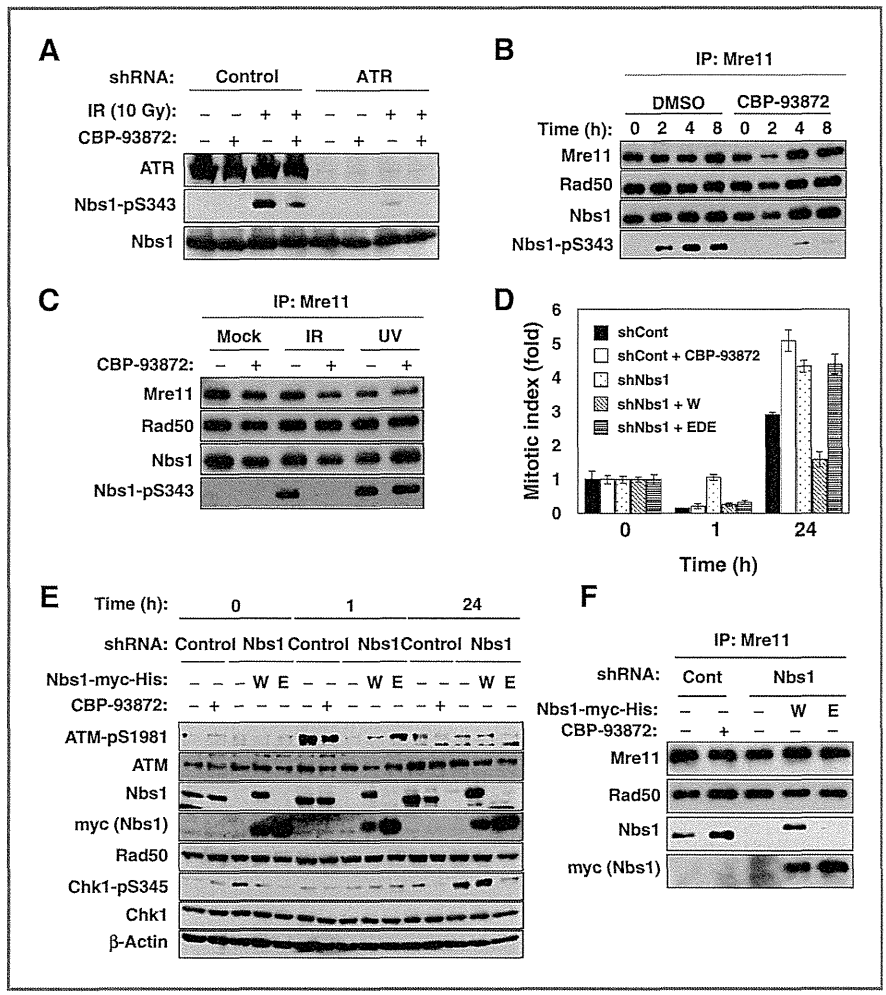

Figure 5. CBP-93872 inhibited ATR-mediated Nbs1 phosphorylation at S343, and a mutant Nbs1 lacking the ability to bind to RPA2 showed a similar G_2 checkpoint abrogation to that with CBP-93872 treatment. A, HT29 cells were infected with Tet-on inducible lentiviruses expressing shControl or shATR. These cells were cultured in the presence of doxycycline (1 μg/mL) for 3 days. Cells were treated with or without IR (10 Gy) in the presence or absence of CBP-93872 (20 μmol/L). Two hours after irradiation, cells were harvested and the chromatin fractions were analyzed by immunoblotting using the indicated antibodies. B, HT29 cells were exposed to IR (10 Gy) in the presence of DMSO (control) or CBP-93872 (20 μmol/L) and harvested at the indicated times. Cell lysates were immunoprecipitated using anti-Mre11 antibodies. The resultant immunoprecipitates were subjected to immunoblotting using the indicated antibodies. C, HT29 cells were mock treated or treated with IR (10 Gy) or UV (100 J/m^2) in the presence or absence of CBP-93872 (20 μmol/L). Cells were harvested 2 hours after IR treatment. Immunoprecipitation and immunoblotting were performed as in B. D, HT29 cells expressing control shRNA (Control) or cells depleted of endogenous Nbs1 (Nbs1) were transfected with plasmids expressing myc-tagged Nbs1, either wild-type (W) or an EDE mutant (E) that lacks the ability to bind to RPA2. Cells were treated with IR and mitotic indices were determined as in Fig. 2A. Data are presented as means ± SD of at least three independent experiments. E, cells were treated with IR (10 Gy) in the presence or absence of CBP-93872 (20 μmol/L). One hour after irradiation, nocodazole (500 nmol/L) was added and cells were harvested at the indicated times. The lysates were subjected to immunoblotting using the indicated antibodies. F, cell lysates from HT29 cells expressing either wild-type or an EDE mutant Nbs1 were immunoprecipitated using anti-Mre11 antibodies. The resultant immunoprecipitates were subjected to immunoblotting using the indicated antibodies.

less cytotoxicity and possess the ability to potentiate the antitumor efficiency of DNA-damaging agents.

Very recently, it was reported that ATR activation following DSB is regulated by two distinct modes (29, 30). After DNA-end resection is initiated, the Rad17–RFC complex recognizes generated ssDNA/dsDNA junctions and subsequently recruits Rad9–Rad1–Hus1 (9-1-1) complexes and TopBP1 onto the junctions. This recruitment leads to the initiation of ATR activation. Continued DNA-end resection results in lengthened ssDNA regions that recruit RPA and ATR-ATRIP. MRN complexes then directly bind to RPA-ssDNA through the EDE domain of Nbs1 and recruit TopBP1, activating ATR-ATRIP. This mode of action seems to function in the amplification and maintenance of ATR checkpoint signaling (32). CBP-93872 specifically inhibited maintenance, but not initiation, of ATR checkpoint signaling, suggesting that it functions in Nbs1-dependent ATR activation (Fig. 6C). Intriguingly, CBP-93872 directly inhibited ssDNA-induced but not ssDNA/dsDNA

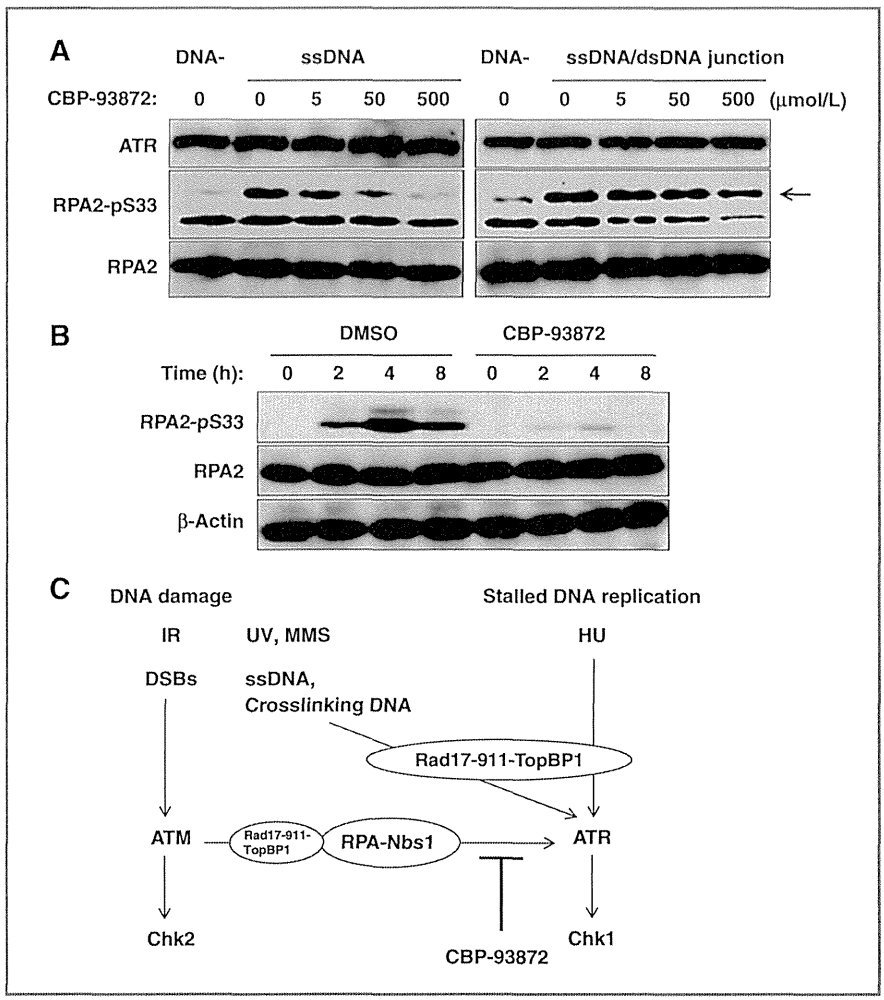

Figure 6. CBP-93872 inhibited ssDNA-dependent ATR activation *in vitro*. A, nuclear extracts prepared from HCT116 cells were incubated with 70nt single-stranded DNA (ssDNA) or ssDNA/dsDNA junction produced by annealing 70nt ssDNA with 50nt ssDNA at 37°C for 15 minutes. The extracts were then subjected to immunoblotting and phosphorylation of RPA2 pS33 was detected with the specific antibodies. The arrows indicate phosphorylation bands of RPA2 at S33. B, HT29 cells were treated with IR (10 Gy) in the presence of DMSO or CBP-93872 (20 μmol/L). Cells were harvested at the indicated times and the lysates were subjected to immunoblotting using the indicated antibodies. C, schematical presentation of the molecular basis underlying checkpoint inhibition by CBP-93872. ATR activation following DSB is regulated by two distinct modes. After DNA-end resection is initiated, Rad17-(9-1-1)-TopBP1 leads to the initiation of ATR activation. Continued DNA-end resection recruits RPA–Nbs1 complexes and further activates ATR. ATR activation following ssDNA or cross-linking DNA generated by DNA damage or stalled DNA replication is mainly mediated by the Rad17-(9-1-1)-TopBP1 axis independently of Nbs1. In this way, CBP-93872 specifically inhibits Nbs1-dependent ATR activation.

junction activation of ATR *in vitro*. Consistent with this, treatment with CBP-93872 suppressed ATR-dependent Nbs1 phosphorylation at S343 and RPA2 phosphorylation at S33.

In conclusion, although the detailed mechanism underlying inhibition of ssDNA-induced ATR activation by CBP-93872, including its structural basis, remains elusive, our results showed that ssDNA-induced ATR activation is a promising molecular target for a G_2 checkpoint inhibitor that specifically sensitizes p53-mutated cancer cells to DSB-inducing DNA damage therapy.

Disclosure of Potential Conflicts of Interest

No potential conflicts of interest were disclosed.

Authors' Contributions

Conception and design: M. Nakanishi
Development of methodology: T. Hirokawa
Acquisition of data (provided animals, acquired and managed patients, provided facilities, etc.): T. Hirokawa, B. Shiotani, K. Murata, Y. Johmura, M. Haruta
Analysis and interpretation of data (e.g., statistical analysis, biostatistics, computational analysis): T. Hirokawa, B. Shiotani, M. Shimada, K. Murata, M. Haruta, H. Tahara, H. Takeyama
Writing, review, and/or revision of the manuscript: T. Hirokawa, M. Nakanishi
Administrative, technical, or material support (i.e., reporting or organizing data, constructing databases): B. Shiotani, M. Shimada, M. Nakanishi
Study supervision: M. Nakanishi

Acknowledgments

The authors thank Dr. N. Harada and Chugai Pharmaceutical Co., Ltd. for providing CBP-93872 and Dr. H. Miyoshi for lentiviral vectors. The authors thank Y. Chiba and C. Yamada-Namikawa for technical assistance.

Grant Support

This work was performed as a research program of the Project for Development of Innovative Research on Cancer Therapeutics (P-DIRECT), Ministry of Education, Culture, Sports, Science and Technology of Japan (M. Nakanishi). This work was also supported by a Grant-in-Aid for Scientific Research on Innovative Area "Cell fate control," Scientific Research (A), and Challenging Exploratory Research from the Ministry of Education, Culture, Sports, Science and Technology of Japan (M. Nakanishi).

The costs of publication of this article were defrayed in part by the payment of page charges. This article must therefore be hereby marked *advertisement* in accordance with 18 U.S.C. Section 1734 solely to indicate this fact.

Received December 20, 2013; revised April 10, 2014; accepted April 17, 2014; published OnlineFirst May 29, 2014.

References

1. Harper JW, Elledge SJ. The DNA damage response: ten years after. Mol Cell 2007;28:739–45.
2. Canman CE, Lim DS, Cimprich KA, Taya Y, Sakaguchi K, Appela E, et al. Activation of the ATM kinase by ionizing radiation and phosphorylation of p53. Science 1998;281:1677–9.
3. Mirzayans R, Andrais B, Scott A, Murray D. New insights into p53 signaling and cancer cell response to DNA damage: implications for cancer therapy. J Biomed Biotechnol 2012;2012:170325.
4. Zhao H, Piwnica-Worms H. ATR-mediated checkpoint pathways regulate phosphorylation and activation of human Chk1. Mol Cell Biol 2001;21:4129–39.
5. Zhao H, Watkins JL, Piwnica-Worms H. Disruption of the checkpoint kinase 1/cell division cycle 25A pathway abrogates ionizing radiation-induced S and G2 checkpoints. Proc Natl Acad Sci U S A 2002;99:14795–800.
6. Bartek J, Lukas J. Pathways governing G1/S transition and their response to DNA damage. FEBS Lett 2001;490:117–22.
7. Löbrich M, Jeggo PA. The impact of a negligent G2/M checkpoint on genomic instability and cancer induction. Nat Rev Cancer 2007;7:861–869.
8. Niida H, Nakanishi M. DNA damage checkpoints in mammals. Mutagenesis 2006;21:3–9.
9. Shiloh Y. ATM and related protein kinases: safeguarding genome integrity. Nat Rev Cancer 2003;3:155–68.
10. Burma S, Chen DJ. Role of DNA-PK in the cellular response to DNA double-strand breaks. DNA Repair (Amst) 2004;3:909–18.
11. Jazayeri A, Falck J, Lukas C, Bartek J, Smith GC, Lukas J, et al. ATM- and cell cycle-dependent regulation of ATR in response to DNA double-strand breaks. Nature Cell Biology 2006;8:37–45.
12. Flynn RL, Zou L. ATR: a master conductor of cellular responses to DNA replication stress. Trends Biochem Sci 2011;36:133–40.
13. Zou L, Elledge SJ. Sensing DNA damage through ATRIP recognition of RPA-ssDNA complexes. Science 2003;300:1542–8.
14. Graves PR, Yu L, Schwarz JK, Gales J, Sausville EA, O'Connor PM, et al. The Chk1 protein kinase and the Cdc25C regulatory pathways are targets of the anticancer agent UCN-01. J Biol Chem 2000;275:5600–5.
15. Syljuåsen RG, Sørensen CS, Nylandsted J, Lukas C, Lukas J, Bartek J. Inhibition of Chk1 by CEP-3891 accelerates mitotic nuclear fragmentation in response to ionizing Radiation. Cancer Res 2004;64:9035–40.
16. Ashwell S, Janetka JW, Zabludoff S. Keeping checkpoint kinases in line: new selective inhibitors in clinical trials. Expert Opin Investig Drugs 2008;17:1331–40.
17. Takai H, Tominaga K, Motoyama N, Minamishima YA, Nagahama H, Tsukiyama T, et al. Aberrant cell cycle checkpoint function and early embryonic death in Chk1(−/−) mice. Genes Dev 2000;14:1439–47.
18. Liu Q, Guntuku S, Cui XS, Matsuoka S, Cortez D, Tamai K, et al. Chk1 is an essential kinase that is regulated by Atr and required for the G(2)/M DNA damage checkpoint. Gene Dev 2000;14:1448–59.
19. Brown EJ, Baltimore D. ATR disruption leads to chromosomal fragmentation and early embryonic lethality. Genes Dev 2000;14:397–402.
20. de Klein A, Muijtjens M, van Os R, Verhoeven Y, Smit B, Carr AM, et al. Targeted disruption of the cell-cycle checkpoint gene ATR leads to early embryonic lethality in mice. Curr Biol 2000;10:479–82.
21. Cimprich KA, Cortez D. ATR: an essential regulator of genome integrity. Nat Rev Mol Cell Biol 2008;9:616–27.
22. Xu Y, Ashley T, Brainerd EE, Bronson RT, Meyn MS, Baltimore D. Targeted disruption of ATM leads to growth retardation, chromosomal fragmentation during meiosis, immune defects, and thymic lymphoma. Genes Dev 1996;10:2411–22.
23. Harada N, Watanabe Y, Yoshimura Y, Sakumoto H, Makishima F, Tsuchiya M, et al. Identification of a checkpoint modulator with synthetic lethality to p53 mutants. Anticancer Drugs 2011;22:986–94.
24. Shimada M, Niida H, Zineldeen DH, Tagami H, Tanaka M, Saito H, et al. Chk1 is a histone H3 threonine 11 kinase that regulates DNA damage-induced transcriptional repression. Cell 2008;132:221–32.
25. Liu S, Shiotani B, Lahiri M, Maréchal A, Tse A, Leung CC, et al. ATR autophosphorylation as a molecular switch for checkpoint activation. Mol Cell 2011;43:192–202.
26. Shiotani B, Zou L. Single-stranded DNA orchestrates an ATM-to-ATR switch at DNA breaks. Mol Cell 2009;33:547–58.
27. Sartori AA, Lukas C, Coates J, Mistrik M, Fu S, Bartek J, et al. Human CtIP promotes DNA end resection. Nature 2007;450:509–14.
28. Huertas P, Jackson SP. Human CtIP mediates cell cycle control of DNA end resection and double strand break repair. J Biol Chem 2009;284:9558–65.
29. Shiotani B, Nguyen HD, Håkansson P, Maréchal A, Tse A, Tahara H, et al. Two distinct modes of ATR activation orchestrated by Rad17 and Nbs1. Cell Rep 2013;3:1651–62.
30. Duursma AM, Driscoll R, Elias JE, Cimprich KA. A role for the MRN complex in ATR activation via TOPBP1 recruitment. Mol Cell 2013;50:116–22.
31. Do K, Doroshow JH, Kummar S. Wee1 kinase as a target for cancer therapy. Cell Cycle 2013;12:3159–64.
32. Kousholt AN, Fugger K, Hoffmann S, Larsen BD, Menzel T, Sartori AA, et al. CtIP-dependent DNA resection is required for DNA damage checkpoint maintenance but not initiation. J Cell Biol 2012;197:869–76.